

AD-A272 659



WL-TR-93-2046

LASER DIAGNOSTICS OF RF HYDROGEN
PLASMA REACTORS: APPLICATION TO THE
PROCESSING OF III-V MATERIALS



B. L. PREPPERNAU, A. TSEREPI, J. DUNLOP, AND T. A. MILLER

DEPARTMENT OF CHEMISTRY
OHIO STATE UNIVERSITY
COLUMBUS OHIO 43210

FEBRUARY 1993

DTIC
ELECTE
NOV 15 1993
S E D

FINAL REPORT FOR PERIOD JULY 1989 - SEPTEMBER 1992

Approved for public release; distribution unlimited.

AERO PROPULSION AND POWER DIRECTORATE
WRIGHT LABORATORY
AIR FORCE SYSTEMS COMMAND
WRIGHT-PATTERSON AIR FORCE BASE, OH 45433-6563

93-27800

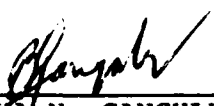
00 05


NOTICE

When Government drawings, specifications, or other data are used for any purpose other than in connection with a definitely Government-related procurement, the United States Government incurs no responsibility or any obligation whatsoever. The fact that the government may have formulated or in any way supplied the said drawings, specifications, or other data, is not to be regarded by implication, or otherwise in any manner construed, as licensing the holder, or any other person or corporation; or as conveying any rights or permission to manufacture, use, or sell any patented invention that may in any way be related thereto.

This report is releasable to the National Technical Information Service (NTIS). At NTIS, it will be available to the general public, including foreign nations.

This technical report has been reviewed and is approved for publication.


BISWA N. GANGULY
Research Physicist
Power Components Branch
Aerospace Power Division
Aero Propulsion and Power Directorate


JOSEPH A. WEIMER, Act Chief
Power Components Branch
Aerospace Power Division
Aero Propulsion & Power Directorate


WILLIAM U. BORGER
Chief, Aerospace Power Division
Aero Propulsion & Power Directorate

If your address has changed, if you wish to be removed from our mailing list, or if the addressee is no longer employed by your organization please notify WL/POOC, WPAFB, OH 45433-6563 to help us maintain a current mailing list.

Copies of this report should not be returned unless return is required by security considerations, contractual obligations, or notice on a specific document.

REPORT DOCUMENTATION PAGE			Form Approved OMB No 0704-0188	
<small>Public reporting burden for this collection of information is estimated to average 1 hour per response, including the time for reviewing instructions, searching existing data sources, gathering and maintaining the data needed, and completing and reviewing the collection of information. Send comments regarding this burden estimate or any other aspect of this collection of information, including suggestions for reducing this burden, to Washington Headquarters Services, Directorate for Information Operations and Reports, 1215 Jefferson Davis Highway, Suite 1204, Arlington, VA 22202-4302, and to the Office of Management and Budget, Paperwork Reduction Project (0704-0188), Washington, DC 20503.</small>				
1. AGENCY USE ONLY (Leave blank)	2. REPORT DATE February 1993	3. REPORT TYPE AND DATES COVERED Final July 89-Sep 92		
4. TITLE AND SUBTITLE Laser Diagnostics of RF Hydrogen Plasma Reactors: Applications to the Processing of III-V Materials		5. FUNDING NUMBERS C: F33615-89-C-2921 PE: 61102F PR 2301 TA S1 WU 40		
6. AUTHOR(S) B.L. Preppernau, A. Tserepi, J. Dunlop, and T.A. Miller				
7. PERFORMING ORGANIZATION NAME(S) AND ADDRESS(ES) Dept of Chemistry Ohio State University Columbus OH 43210		8. PERFORMING ORGANIZATION REPORT NUMBER		
9. SPONSORING/MONITORING AGENCY NAME(S) AND ADDRESS(ES) Aero Propulsion and Power Directorate Wright Laboratory Air Force Materiel Command Wright Patterson AFB, OH 45433-7650		10. SPONSORING/MONITORING AGENCY REPORT NUMBER WL-TR-93-2046		
11. SUPPLEMENTARY NOTES				
12a. DISTRIBUTION / AVAILABILITY STATEMENT approved for public; distribution is unlimited		12b. DISTRIBUTION CODE		
13. ABSTRACT (Maximum 200 words) Two photon laser induced fluorescence (TALIF) has been developed as a convenient and reliable diagnostic of H atoms in plasma processing environments. It has high spatial and temporal resolution, good sensitivity, and the capability of absolute concentration measurements. Detailed diagnostics have been carried out in plasma reactors with and without semiconducting wafers. These measurements have led to a model that incorporates H atom production, diffusion, and surface recombination. This model has accurately predicted both the spatial and temporal behavior of the H-atom concentration in a plasma processing environment.				
14. SUBJECT TERMS Atomic H, glow discharge, plasma processing, laser diagnostics III-V semiconductors		15. NUMBER OF PAGES 69		
		16. PRICE CODE		
17. SECURITY CLASSIFICATION OF REPORT unclass	18. SECURITY CLASSIFICATION OF THIS PAGE unclass	19. SECURITY CLASSIFICATION OF ABSTRACT unclass	20. LIMITATION OF ABSTRACT UL	

PREFACE

This report covers work performed during the period between July 1, 1989-September 28, 1992 under contract F33615-89-C-2921. The contract was administered under the direction of the Wright Laboratory, Aero Propulsion and Power Directorate, Wright Patterson AFB, Ohio, with Dr. Bish Ganguly, Research Physicist, acting as project monitor. Parts of this report cover work performed for the Ph.D. degree by Bryan Preppernau and Angeliki Tserepi. Jim Dunlop contributed to this work as a postdoctoral student. B. Preppernau and Jim Dunlop are now employed by Sandia Laboratories, at Albuquerque, New Mexico and Livermore, California respectively. Angeliki Tserepi is expected to finish her Ph.D. degree in 1993.

Accession For	
NTIS	CRA&I <input checked="" type="checkbox"/>
DTIC	TAB <input checked="" type="checkbox"/>
Unannounced	<input type="checkbox"/>
Justification	
By	
Distribution /	
Availability Codes	
Dist	Avail and/or Special
A-1	

DTIC QUALITY INSPECTED 8

TABLE OF CONTENTS

1.	INTRODUCTION	1
2.	EXPERIMENTAL DETAILS	4
	A. LASER CONFIGURATION	4
	B. SIGNAL DETECTION AND ANALYSIS	6
	C. H-ATOM CONCENTRATION CALIBRATION PROCEDURE	10
3.	H-ATOM DIAGNOSTIC RESULTS	16
	A. H-ATOM DEPENDENCE UPON DISCHARGE PARAMETERS	16
	B. H-ATOM PROFILES IN UNLOADED DISCHARGES	23
	i) Observations in continuous and pulsed discharges	23
	ii) Model	29
	C. H-ATOM PROFILES IN LOADED DISCHARGES	33
	i) Experimental observations	33
	ii) Model	39
	D. LINEWIDTHS AS A PROBE OF DISCHARGE TEMPERATURE AND PURITY	42
	i) Theory	44
	ii) H ₂ Discharge	44
	iii) Ammonia	49
	iv) Other Processing Gas Plasmas	54
4.	CONCLUSIONS	57
5.	LIST OF REFERENCES	58
	APPENDIX	60

LIST OF ILLUSTRATIONS

- 1) Schematic for production of 205-nm light for H-atom TALIF excitation and detection. Note that the photomultiplier (PMT) is looking perpendicular to the 205-nm beam even though it is depicted in the plane of the figure. 5
- 2) Experimental H-atom TALIF signal trace at 205 nm. Signal acquired under conditions of 0° relative to RF phase, 1 torr H_2 , 13 W RF power at 200 kHz. . . . 9
- 3) Schematic of apparatus used for titration of H-atoms. 12
- 4) Absolute calibration curve of TALIF intensity, Inset: typical titration data show a linear decrease of the TALIF intensity upon addition of NO_2 in the flow reactor. The NO_2 concentration at the x-intercept equals the H-concentration corresponding to the TALIF intensity at the y-intercept. The H-concentrations are then plotted against the observed LIF intensity in the main plot to obtain the calibration curve. 14
- 5) Experimental H-atom TALIF signal response as a function of incident 205-nm laser pulse energy. The curve is a quadratic polynomial regression fit to the measured data. 1 Torr H_2 , 13 W, 100 kHz. 17
- 6) TALIF signal for hydrogen and deuterium gas discharges as a function of RF discharge load power. 1 Torr, 100 kHz, \circ : H_2 , and \bullet : D_2 18
- 7) TALIF signal for hydrogen and deuterium gas discharges as a function of discharge cell pressure. 14 W, 100 kHz, \circ : H_2 , and \bullet : D_2 20
- 8) Ground-state H-atom concentration phase response. The upper trace is the TALIF signal and the lower trace shows the relative response of the PIE over a complete RF cycle. 21
- 9) H-atom TALIF signal versus H_2 concentration in helium. The total discharge cell pressure is 1 Torr. The inset shows an expanded portion of the plot for concentrations below 10%. 22
- 10) Typical H-atom concentration vs distance from the grounded electrode in a 10-MHz continuous discharge. The pressure of pure H_2 was 3 Torr and the power was 10 W. The ground and powered electrode positions are 0 and 19 mm. The solid line represents a fit obtained from the model discussed in the text. 24
- 11) Temporal evolution of H-atom spatial profiles in a pulsed discharge; experimental

	data points and simulated results (solid lines) at $t=0.25$, 1.0 , and 2.5 ms. The pressure was maintained at 3 Torr and the power was 5 W.	26
12)	Decay of H-atom spatial distribution after switching the discharge off; experimental data points and simulated results (solid lines) at elapsed time $t=0.25$, 0.5 , and 1.0 ms after the discharge is turned off. Discharge conditions the same as in Fig. 11.	27
13)	Temporal profile of H-atom concentration taken in the afterglow of a 2-ms pulse discharge at the center of the interelectrode space. A single exponential (as shown by log plot) can fit well the decay of H-concentration at times $\geq 200\mu\text{s}$ after the discharge pulse ends. Discharge conditions as in Fig. 10.	28
14)	Steady-state concentrations for H- and D-atoms at small distances from the stainless steel electrode surface. The solid lines are fits obtained for surfaces with a loss coefficient $\gamma_s=5\%$ for hydrogen and deuterium atoms. Discharge conditions the same as in Fig. 10.	34
15)	Comparison of radial profiles of H-atom concentration probed 1 mm above (a) a GaAs wafer, (b) a stainless-steel substrate, and (c) a gold coated GaAs wafer. Al wafers of $10\times 10\times 0.5$ mm size are centered on the stainless-steel ground electrode extending from -25 mm to $+25$ mm of the x -axis.	35
16)	Evolution of H-atom spatial distribution in a pulsed discharge loaded with a GaAs wafer on the grounded electrode; experimental data points and simulated results (solid and dashed lines) at $t=0.15$ ms, $t=0.50$ ms, and $t=2.50$ ms. The location of the ground and powered electrodes is a 0 and 19 mm, respectively. Discharge conditions: pressure of 3 Torr, and power of 40 W.	37
17)	H-atom concentration vs. distance from the grounded electrode in a continuous discharge: (a) unloaded, loaded with (b) a Si wafer, and (c) a GaAs wafer placed on the grounded electrode (0–0.5 mm). The solid and dashed lines represent fits obtained from a diffusion model. Discharge conditions: pressure of 3 Torr, and power of 10 W.	38
18)	Etalon narrowed TALIF scan of the H atom $3^2\text{S}(^2\text{D})\leftrightarrow 1^2\text{S}(97,492.3\text{ cm}^{-1})$ transition from atoms generated in an RF discharge. Actual data points and a Gaussian fit to the data are presented.	47
19)	Comparison of linewidth dependence on H_2 pressure (recorded at 12 W RF power) and on discharge power (recorded at an H_2 pressure of 0.42 Torr). Also shown is the temperature scale corresponding to the observed linewidths.	48
20)	Comparison of the linewidth of RF generated H-atoms (inner trace) and atoms	

	generated from the photodissociation of ammonia. Actual data points and Gaussian fits are shown.	50
21)	Dependence of signal intensity on laser power for RF and photodissociation-generated H-atoms. A slope of 2 is predicted for two-photon TALIF, and a slope of 3 is predicted for the dissociating photon plus the subsequent TALIF detection. Notice the saturation effect at higher laser powers for the NH_3 -generated signals.	53
22)	Comparison of the lineshapes for TALIF signals produced from photodissociation of acetylene (triangles) and H_2S	55

SECTION 1

INTRODUCTION

The active and downstream plasma processing of semiconductor devices and surface modification of aerospace materials is fundamental to Air Force and other DOD applications. There is a great need for a more *fundamental understanding* of these sorts of cold, reactive plasmas. There is also a need for the development of *practical diagnostics* for plasmas actually used or potentially of use in materials processing. Of these techniques, laser diagnostics are almost certainly among the most powerful and promising.

A particularly striking confluence of fundamental and applied interests occurs with the use of H_2 plasmas in the processing of III-V electronic devices. On the fundamental side, there is probably no system with simpler atomic and molecular species. On the other hand, the H_2 system exhibits all the properties of typical reactive plasmas. The obtainment of a good fundamental understanding of the H_2 RF plasma would seem a necessary prelude to the complete understanding of more complex plasma systems.

However, just as importantly, the H_2 plasma has immediate application in the processing of III-V materials. Thus, there is every reason to believe that these same diagnostic techniques can be applied to elucidate the mechanisms of the processing of III-V materials in H_2 plasmas or other plasmas containing hydrogenic species. Ultimately, this diagnostic may provide a unique approach to understanding the plasma induced surface chemistry in these systems. While a basic knowledge of the plasma processes is a necessary prerequisite for a complete understanding of these systems, it should be possible to make *concurrent* progress in controlling and manipulating plasma processing by applying laser diagnostics while these diagnostics

themselves are in development.

H_2 and H_2/CH_4 plasmas are used to directly etch GaAs and also InP.¹ Of at least comparable interest is the use of H_2 plasmas to passivate devices. For example, while other etchant gases, e.g. Cl_2 , appear at the moment preferable for etching some III-V materials, e.g. GaAlAs, passivation in an H_2 plasma of surface defects created in other etching processes, seems very effective.² Moreover, device structures can be produced by selective (using masks) H_2 passivation of dopants. Examples include the production of a variety of GaAs FET with a hydrogenated channel³ and stripe geometry AlGaAs-GaAs quantum well lasers using masked hydrogenation to produce current guiding through the heterostructure.⁴

Unintentional, sometimes deleterious, hydrogenation can also occur in processing environments. For example, H_2 fluorocarbon mixtures are sometimes used for etching SiO_2 and SiN_x layers on III-V semiconductors.⁵ Even "accidents" such as introduction of moisture into a plasma can lead to H-atom production.

The report describes the systematic development of a reliable and accurate diagnostic for probing of the most abundant reactive species in a cold, processing hydrogen plasma, the H-atom. The diagnostic provides a spatially ($\approx 100\mu$) and temporally (≈ 10 nsec) resolved relative (≈ 10 percent precision) and absolute (≈ 25 percent precision) measure of the H-atom concentration within the plasma. This diagnostic is based upon the two-photon absorption laser-induced fluorescence (TALIF) technique. It is described in detail in the second section of this report.

As we have developed the diagnostic, we have applied it to an elucidation of the cold H_2 plasmas typical of processing environments. In Section 3 A, we describe the general

dependences of the H-atom concentration on discharge parameters. In Section 3.B, we report H-atom spatial profiles in continuous and pulsed H_2 discharges. We further present a model of the H-atom production and concentration evolution that is in strikingly good agreement with the measured profiles. We then further simulate a processing environment by introducing GaAs and Si wafers into the reactor and observing the modifications caused thereby to the H-atom concentrations. The H-atom concentration model for an unloaded reactor is extended and successfully describes the situation where wafers are present on the electrode. In Section 3.D, we describe how the TALIF linewidths can be used as a sensitive probe of temperature and gas purity within the reactor.

Section 4 is a short summary of conclusions reached and suggestions for further work. The Appendix lists publications and presentations based upon work supported by this contract.

SECTION 2

EXPERIMENTAL DETAILS

A. LASER CONFIGURATION

A schematic of the general experimental scheme used for the TALIF H-atom detection is shown in Fig. 1. The schematic layout shows an RF reactor cell power supply system, the laser system, and the associated acquisition and control electronics. The laser light generation configuration will now be described and the acquisition electronics are discussed below.

The TALIF transition for atomic hydrogen is from the $1s^2S_{1/2}$ ground state to the $3d^2D_{5/2,3/2}$ and $3s^2S_{1/2}$ excited states at 97492 cm^{-1} . Both excited state levels are populated due to the energy level degeneracy in hydrogen for different angular momentum states and due to the two-photon absorption selection rule of $\Delta L = 0, \pm 2$.⁶ The transition requires two 205.14-nm photons to excite the atomic ground state. The TALIF transition has also been observed in deuterium at 97519 cm^{-1} in the course of this research.

The excited state is only weakly populated by the discharge impact kinetics due to a rapid ($\approx 15\text{ nsec}$) radiative lifetime. Thus, the TALIF excitation can be expected to effectively alter the population of the upper state and its emission, although significant photon density is required given the small two-photon absorption cross section.

TALIF measurements for H-atoms can be performed using a high pressure H_2 -filled Raman cell for frequency shifting or by sum-frequency mixing (SFM) in a beta-barium borate (BBO) crystal. For our purposes the use of SFM with a BBO crystal is preferred since SFM generates far more than 205-nm light. The light generation scheme depicted in Fig. 1 was used in all but our initial experiments. The probe laser is generated by pumping a Quanta-Ray PDL-2

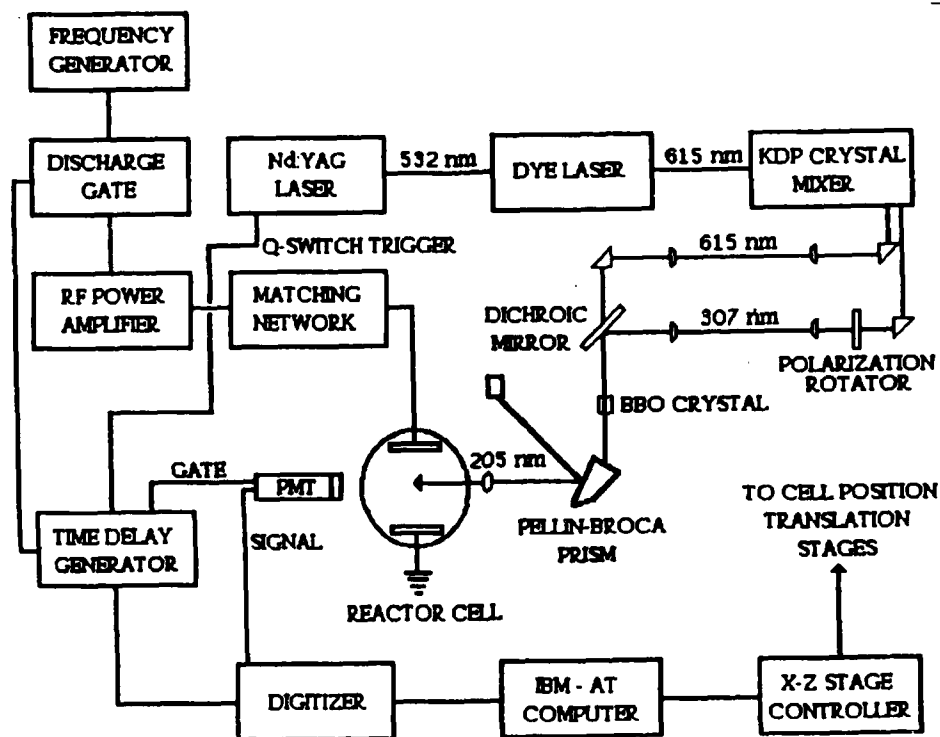


Figure 1. Schematic for production of 205-nm light for H-atom TALIF excitation and detection. Note that the photomultiplier (PMT) is looking perpendicular to the 205-nm beam even though it is depicted in the plane of the figure.

dye laser with the second-harmonic 532-nm output of a Quanta-Ray DCR-2A Nd:YAG laser operating at 20 Hz. The dye laser operates with Exciton Sulforhodamine 640 dye at 615 nm. The dye laser output is frequency doubled using a Quanta-Ray WEX KDP crystal providing an output of 7 mJ/pulse at 307 nm and a residual 14 mJ/pulse at 615 nm. Upon exiting the WEX system, the polarization of the 307-nm beam is rotated to coincide with the polarization of the 615-nm beam. Both beams are collimated with a 3:1 telescope and combined via a dichroic mirror. The collinear, collimated beams are input to the BBO crystal manually angle tuned to provide SFG at 205 nm. The spot size diameter of the input beams is 3 mm. The SFG output from the BBO crystal can be as high as 800 microJoules/pulse with careful alignment and overlap of the two input beams. The output pulse energy is carefully measured with a calibrated Molelectron Model J3-05 Joulemeter. Using the BBO SFM technique gives over 10 times the output of the H₂ Raman shift technique. The conversion efficiency of BBO at this wavelength has been quoted possibly as high as 12 percent in the literature⁷, and the efficiency of our system was measured at 11 percent which is predominantly dictated by the input beams profile quality and alignment. Upon leaving the BBO crystal the residual input pump beams are dispersed by a Pellin-Broca prism and beam dumped. The TALIF probe beam is tightly focused by a quartz lens through a Suprasil 1 quartz window into the discharge reactor of interest.

B. SIGNAL DETECTION AND ANALYSIS

Refinement and application of the H-atom TALIF diagnostic was performed using a reactor that has a variable gap cylindrical planar electrode design with water-cooled stainless steel or aluminum electrodes. The discharge load power can be measured with a high voltage probe and a current loop detector whose output is acquired on a digital oscilloscope and

multiplication averaged upon waveform transfer to a personal computer. The reactor cell is mounted on a stepper motor positioned X-Z translation stage. See Fig. 1, X is the in-plane direction perpendicular to the laser beam and Z is perpendicular to the plane of the figure. This configuration allows spatial profile measurements as the cell is translated relative to the fixed laser probe focal point as viewed by the fluorescence collection optics.

The excited state fluorescence from the $3d^2D_{3/2,3/2}$ and $3s^2S_{1/2}$ levels to the $2p^2P_{3/2,1/2}$ on the Balmer alpha line (656.3 nm) transition is detected perpendicular to the primary discharge cell axis and the laser probe beam with focused collection optics. The TALIF passes through a 10-nm FWHM interference filter centered at 656 nm and focused on the photocathode of an ITT Model 4123 gated photomultiplier tube (GPMT). Detection of H-atom TALIF is also easily achieved (provided the average DC current does not exceed the rating of the particular photomultiplier tube) by using continuous (CW) photomultipliers such as the RCA 1P28 or Thorn-EMI 9659 tubes.

The signal collected by either a GPMT or CW photomultiplier is fed directly to the input Tektronix DSA 601 Digital Signal Analyzer or other similar high-speed digital oscilloscope. The data acquisition, dye laser tuning, and experiment timing is controlled by a Stanford research System Digital Delay Generator in combination with an IBM-compatible 386 personal computer. The experiment timing sequence allows for temporally-dependent measurements of H-atom TALIF over all relative phases of the RF discharge driving cycle. The use of a GPMT and a narrow-band interference filter in the collection optics allows detection of the TALIF response even in the presence of the bright plasma-induced emission (PIE). In working with the larger reactor systems it was found that even using a CW photomultiplier was

sufficient provided the anode current of the tube was carefully monitored and did not exceed the maximum rating.

A representative H-atom TALIF signal trace is shown in Figure 2. The TALIF resonance transition is shown for a typical set of discharge operating conditions. As shown, the TALIF signal has an excellent signal/noise ratio which is typical of the TALIF signal over all phases of the RF cycle relative to the PIE. The full-width-half-maximum (FWHM) two-photon linewidth of the TALIF resonance is typically $3.5 \pm 1 \text{ cm}^{-1}$. The dye laser linewidth at 615 nm is approximately 0.6 cm^{-1} ; as measured independently by optogalvanic detection of neon and iron transitions in a hollow-cathode glow discharge lamp. Multiplying this by a factor of 6 (third harmonic of 615 nm times two photons) accounts for the FWHM linewidth of the TALIF transition.

Note the associated Doppler linewidth is $<1.0 \text{ cm}^{-1}$ for the two-photon absorption in hydrogen at a neutral atom temperature of 300-500 Kelvin which might be expected in the center of the discharge gap at zero degrees phase angle in the RF current cycle. Thus our TALIF measurements do not have a sufficiently small laser probe linewidth to measure H-atom linewidths with typical thermal energies without etalon narrowing of the dye laser fundamental output.

In some experiments (see Section 3.D) the linewidth of the dye laser was narrowed by an intracavity etalon to $\approx 0.06 \text{ cm}^{-1}$. The dye laser is scanned by pressure tuning, which entails evacuating and pressurizing with dry N_2 a box surrounding the etalon and grating. This system is controlled by a solenoid valve switched by a relay that is actuated by the data acquisition software.

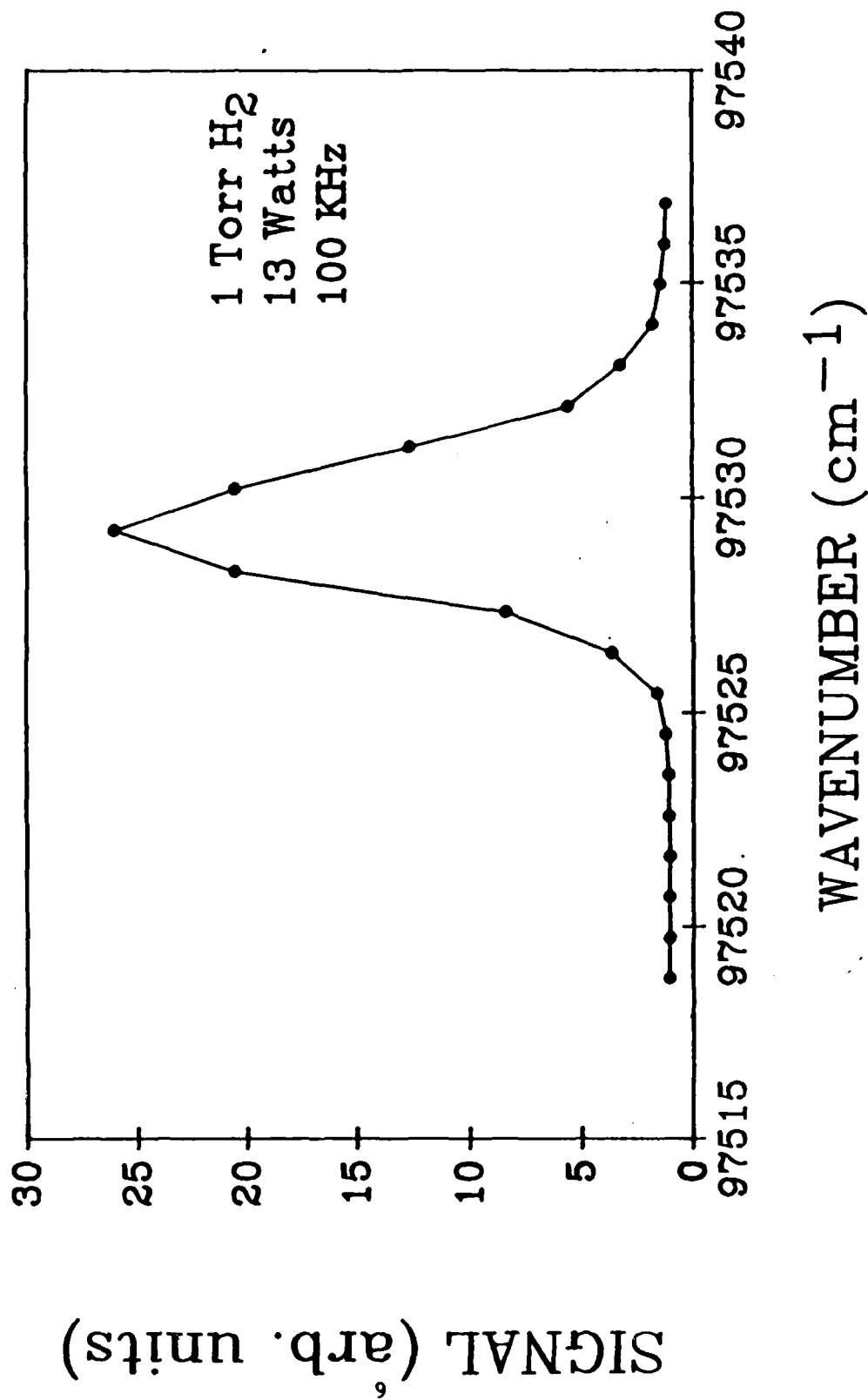


Figure 2. Experimental H-atom TALIF signal trace at 205 nm. Signal acquired under conditions of 0° relative to RF phase, 1 torr H₂, 13 W RF power at 200 kHz.

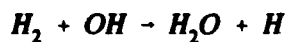
C. H-ATOM CONCENTRATION CALIBRATION PROCEDURE

Having developed a laser diagnostic to detect H-atoms, it would be useful to place the amount of atoms detected on an absolutely calibrated scale and determine actual local concentrations of atoms directly in the plasma. By directing an external source of H-atoms into a central position in the volume of a plasma reactor, the TALIF signal derived from this source can be made to simulate detection of plasma-generated atoms. The external source of atoms, usually generated via microwave discharge, provides a steady, reproducible, and controllable TALIF response. Simultaneously, small quantities of molecules known to efficiently react and combine with the atomic species can be added, and a corresponding decrease in the TALIF signal intensity can be observed as the atoms are depleted. This reaction or titration technique can give a reliable means of determining the concentration of atomic species corresponding to a given amount of TALIF signal.

Calibration of the fluorescence signal collected by the PMT-filter combination was performed using in-situ titration of the H-atoms by chemical reaction with NO_2 . The titration reaction proceeds as⁸



with a reaction rate constant of $k_{298} = 1.3 \times 10^{-10} \text{ cm}^3 \text{ s}^{-1}$ where the rate constant is given for room temperature ($T=298\text{K}$). There is also a secondary reaction of OH with H_2 given by



with a reaction rate constant $k_{298} = 1.6 \times 10^{-15} \text{ cm}^3 \text{ s}^{-1}$. However, provided the ambient H_2 concentration remains below 1 Torr ($3.3 \times 10^{16} \text{ cm}^{-3}$) this reaction will not appreciably perturb the main reaction. Sufficient mixing time must be allowed to ensure the reaction goes to completion. To have a reaction go to 99 percent completion implies that the mixing time, t_{mix} , must be greater than 5 characteristic reaction times, τ . In other words, the percentage of complete reaction is

$$1 - e^{-t/\tau} = 1 - e^{-5\tau/\tau} = 1 - e^{-5} = 0.9932 = 99\% \quad (1)$$

The characteristic reaction time is the inverse of the reaction rate constant times the concentration of reactants. For example, in the case of the reaction in Equation 1, at the point of complete reaction (here called endpoint) a measured concentration of NO_2 is used to react completely with an equal concentration of H-atoms. If the concentration of $[\text{NO}_2]$ used is $1 \times 10^{15} \text{ cm}^{-3}$, then the required mixing time must be at least

$$t_{\text{mix}} \geq 5\tau = 5(k_{298}[\text{NO}_2])^{-1} = 7.7 \text{ microseconds} \quad (2)$$

In the titration assembly described below, the main gas flow rates are adjusted to reduce the slug flow gas velocity in the mixing zone and raise the mixing time to approximately 4 milliseconds, clearly satisfying the condition in Equation 2.

The titration assembly is shown in Fig. 3. At the side inlet a gas mixture of H_2/Ar is passed through a microwave discharge produced by an air-cooled Evenson microwave discharge cavity which dissociates the molecular gas mixture. The presence of argon helps to

Titration Experiment Apparatus

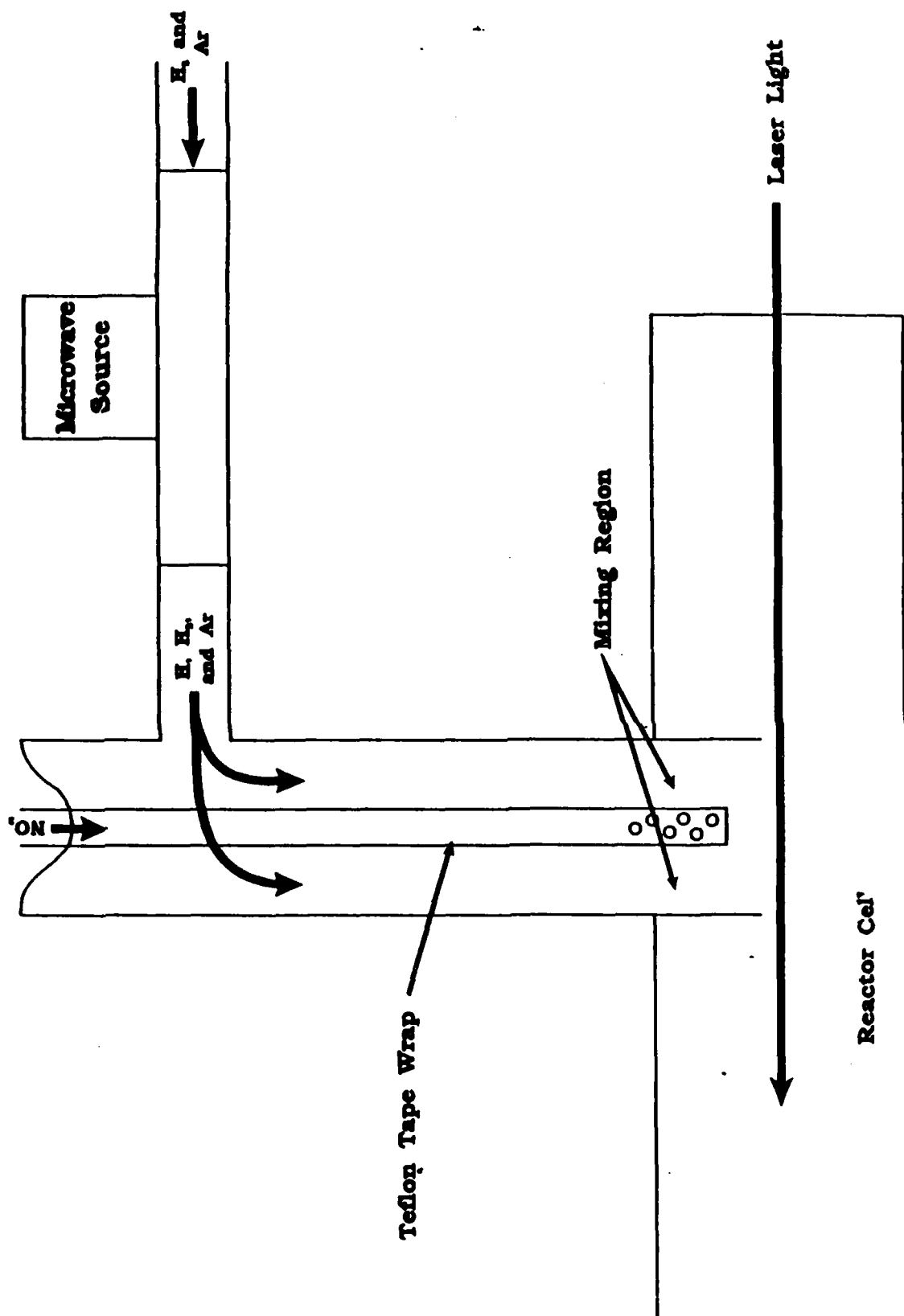


Figure 3. Schematic of apparatus used for titration of H-atoms.

induce more complete dissociation. The discharge section is composed of quartz for both heat resistance and to minimize reactions of the microwave plasma with the walls. Further downstream, NO_2 is introduced through a glass coaxial tube which passes the gas to a perforated mixing zone approximately 2 cm in length and 2 cm in diameter. The inner tube is covered by a Teflon sleeve to reduce the amount of recombination of H-atoms on the tube surface. The assembly is placed through a 3/4 inch diameter (I.D.) Cajon O-Ring fitting welded to a 2-3/4 inch Conflat copper gasket sealed flange. The Conflat flange is mated to a port on a given reactor and the length of the titration assembly allows the exit from the mixing zone to be placed at the center of the reactor and near the focal point of the probe laser. For a titration calibration measurement, a steady-state concentration of H-atom is produced by the microwave cavity discharge source and NO_2 is introduced at known mass flow rates. The TALIF fluorescence is monitored and recorded manually as a function of addition of NO_2 . A typical titration data curve is shown in Fig. 4.

At the endpoint (minimum observable TALIF signal), the total pressure in the reactor is recorded. A straight line is least-squares fit to the first several titration data points, and the exact NO_2 endpoint mass flow rate is extrapolated numerically. Combining this information, we can use the following equation, where at the endpoint

$$[\text{H}]_0 = [\text{NO}_2]_0 = (3.3 \times 10^{16} \text{ cm}^{-3} \text{ Torr}^{-1}) \cdot \left(\frac{F(\text{NO}_2)}{\Sigma F} \right) \cdot P \quad (3)$$

where $[\text{H}]_0$ is the concentration of H-atoms titrated, $[\text{NO}_2]_0$ is the concentration of NO_2 used, $F(\text{NO}_2)$ is the mass flow rate of NO_2 measured in standard cubic centimeters per minute

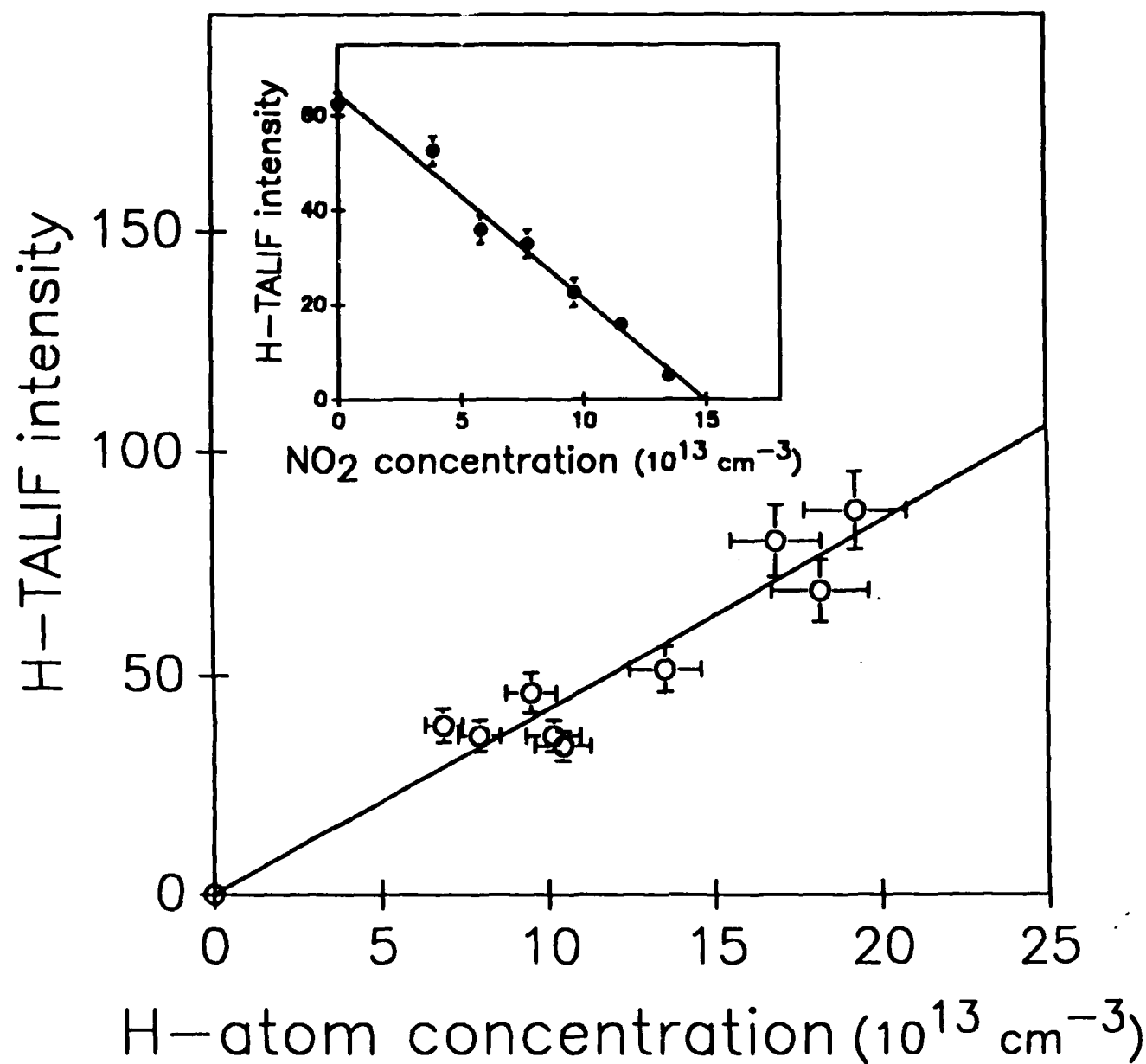


Figure 4. Absolute calibration curve of TALIF intensity, Inset: typical titration data show a linear decrease of the TALIF intensity upon addition of NO_2 in the flow reactor. The NO_2 concentration at the x -intercept equals the H-concentration corresponding to the TALIF intensity at the y -intercept. The H-concentrations are then plotted against the observed LIF intensity in the main plot to obtain the calibration curve.

(sccm), ΣF is the total mass flow rates of all the gases used summed together, and P is the total pressure measured in Torr. The numerical coefficient is used to convert Torr into number density, per cm^3 . Titration curves can be taken for different initial atomic concentrations, PMT gain settings, and probe laser energy. The calibrations curves (see Fig. 4) correlate an experimental TALIF signal with a known concentration. Typically the calibrations are reproducible to 15 percent and believed absolutely accurate to 25 percent. The minimum detectable concentration is extrapolated to be 10^{12} cm^{-3} .

SECTION 3

H-ATOM DIAGNOSTIC RESULTS

A. H-ATOM DEPENDENCE UPON DISCHARGE PARAMETERS

It is useful to get a general overview of the dependence of the TALIF signal upon laser and discharge parameters to characterize its usefulness as a plasma diagnostic. Fig. 5 shows the TALIF signal response as a function of incident 205-nm laser probe pulse energy. The TALIF absorption should depend quadratically upon the laser pulse energy for a fixed interaction volume. The curve through the data points in Fig. 5 is a quadratic polynomial regression fit to the data and shows agreement with the expected TALIF signal response. The lack of a saturation behavior in the data indicates that the TALIF signal response is not affected by competing processes such as multiphoton ionization. In addition, linewidth measurements at zero degrees phase show no power broadening effects for this range of laser pulse energies.

The H-atom TALIF as a function of RF discharge load power is shown in Fig. 6. The TALIF signal has been acquired for both 100% H₂ and D₂ gases at 1 Torr, 50 sccm, 100 kHz RF, and zero degrees RF current phase. The signals shown in Fig. 6 are corrected for differences in laser pulse energies using the data shown in Fig. 5. Interestingly, the deuterium TALIF at 97519 cm⁻¹ shows a factor of 2 decrease relative to the hydrogen TALIF owing either to differences in the D₂ versus H₂ dissociation and recombination rates or the two-photon absorption cross sections. However, both TALIF signals appear to saturate at about 75-W RF power, perhaps due to a saturation of electron-impact dissociation formation of ground state atoms.

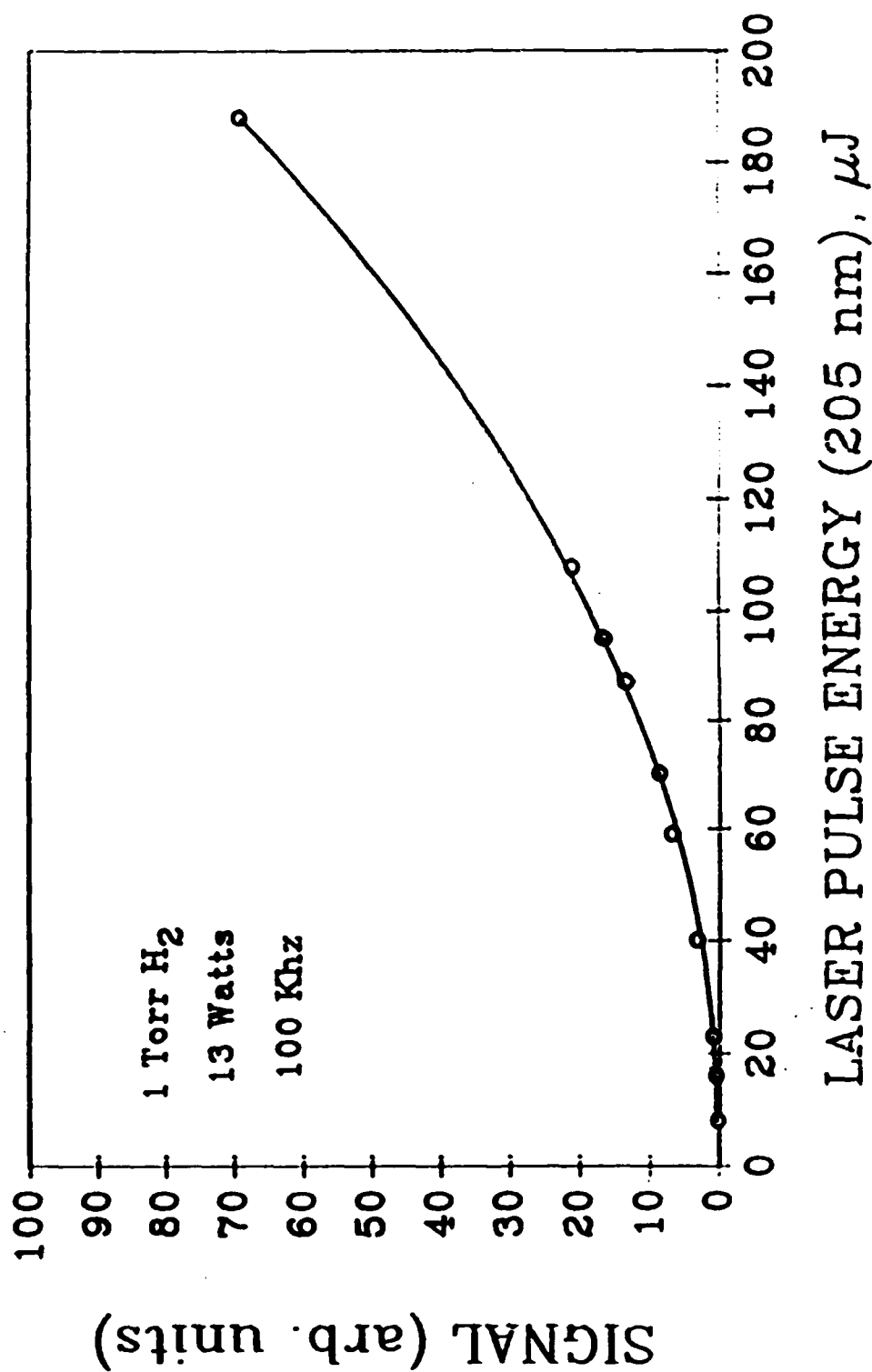


Figure 5. Experimental H-atom TALIF signal response as a function of incident 205-nm laser pulse energy. The curve is a quadratic polynomial regression fit to the measured data. 1 Torr H₂, 13 W, 100 kHz.

TALIF SIGNAL RF POWER DEPENDENCE

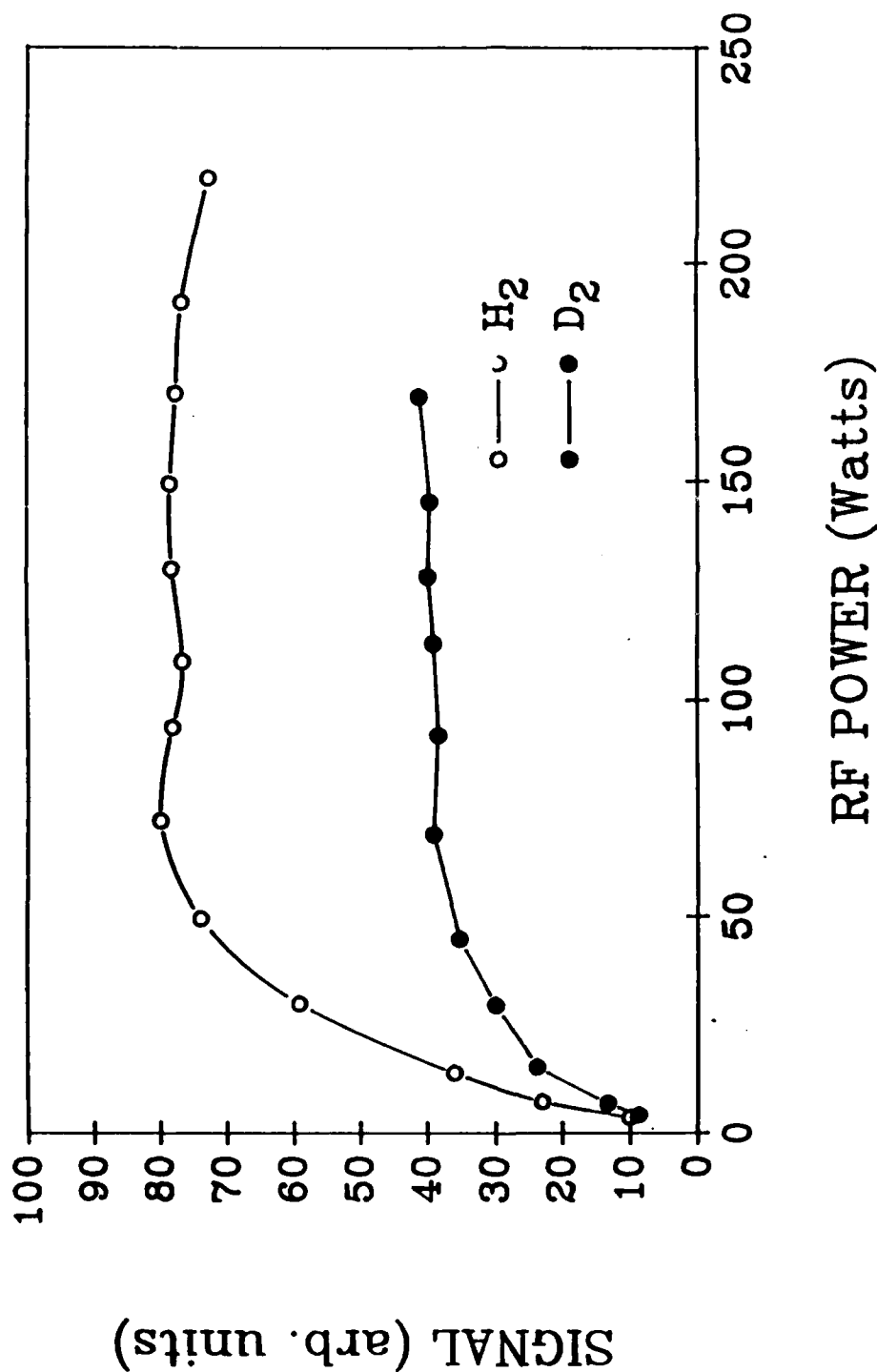


Figure 6. TALIF signal for hydrogen and deuterium gas discharges as a function of RF discharge load power. 1 Torr, 100 kHz.
 \circ : H_2 , and \bullet : D_2 .

The dependence of the TALIF on discharge pressure for hydrogen and deuterium is demonstrated in Fig. 7. Here the RF discharge load power was kept fixed and both TALIF signals normalized to the same 205 nm laser pulse energy. The TALIF has a rapid increase from 0.2 Torr to a maximum at about 1.75 Torr followed by a slow decline through 10 Torr. Both the H₂ and D₂ TALIF show comparable behavior with the signal response following the maximum being interpreted as a loss of fluorescence due to excited state quenching and/or an increase in atom recombination losses as the collision frequency increases with the higher pressures.

The phase dependence of the H atom concentration at 100 kHz is shown in Fig. 8. The data were taken in the middle of the electrode gap at 1.0 Torr of 50 percent hydrogen-50 percent helium and 6-W load power. The upper trace is the TALIF signal; the response is constant within experimental error over all phase angles. No phase dependence was observed even for frequencies as low as 20 kHz; this implies the H atom ground-state lifetime in these discharges is greater than 50 μ sec. The lower trace is the relative response of the PIE over the cycle. A crucial point in making this measurement is the necessity of ensuring that the GPMT does not saturate at phases when the PIE is very bright. This means that the GPMT must be run at a low gain (10^2 - 10^3) in order to achieve a linear response from the GPMT. Indeed, in Fig. 8, at just about the level of experimental uncertainty, there appears to be a very small dip in the TALIF signal at the maximum of the PIE, presumably due to an incipient saturation effect.

The H-atom TALIF signal versus H₂ concentration in helium is shown in Fig. 9. The TALIF signal is nonlinear over most of the H₂ percentage concentrations. However, the inset

TALIF SIGNAL PRESSURE DEPENDENCE

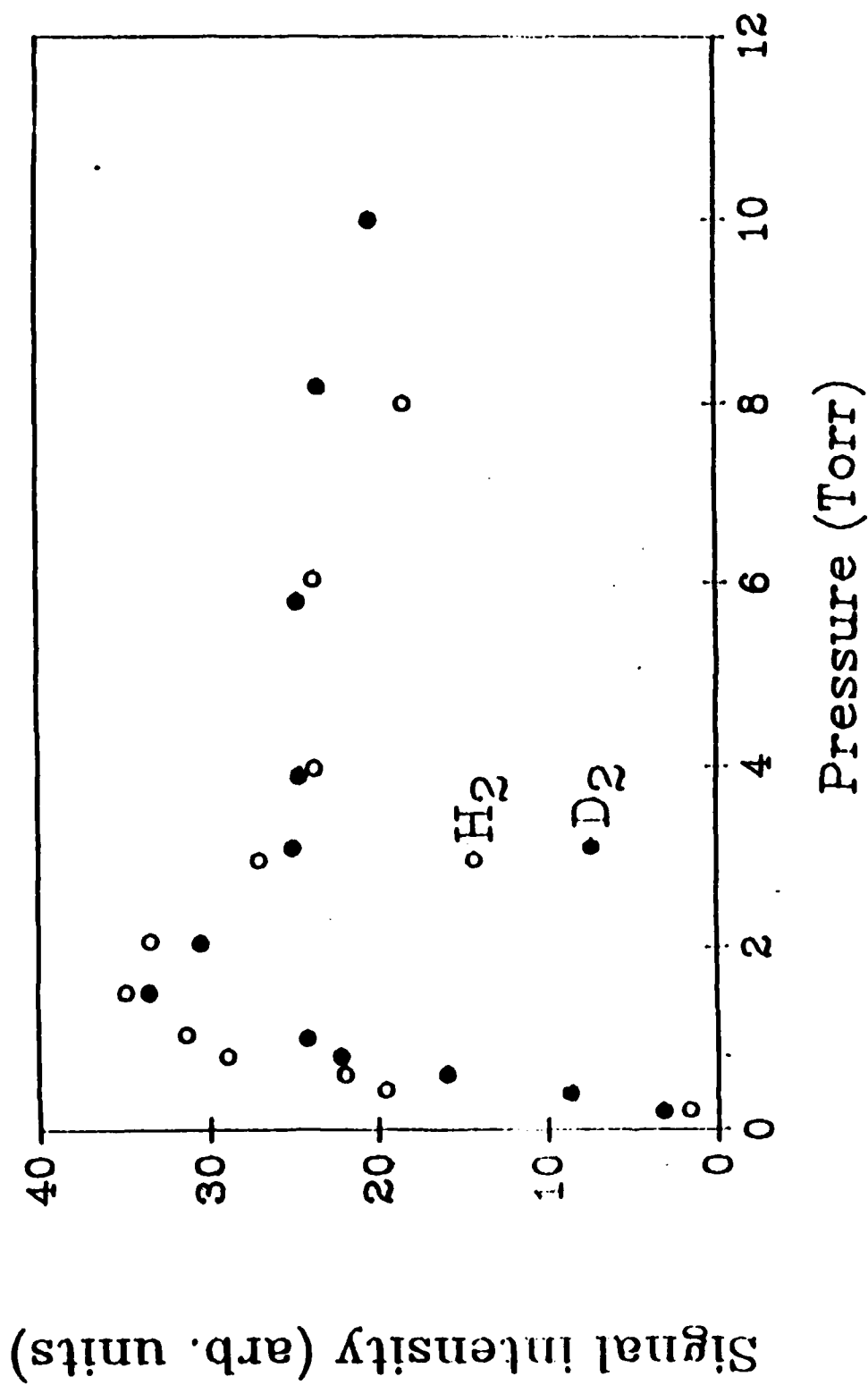


Figure 7. TALIF signal for hydrogen and deuterium gas discharges as a function of discharge cell pressure. 14 W, 100 kHz.
 ○: H_2 , and ●: D_2 .

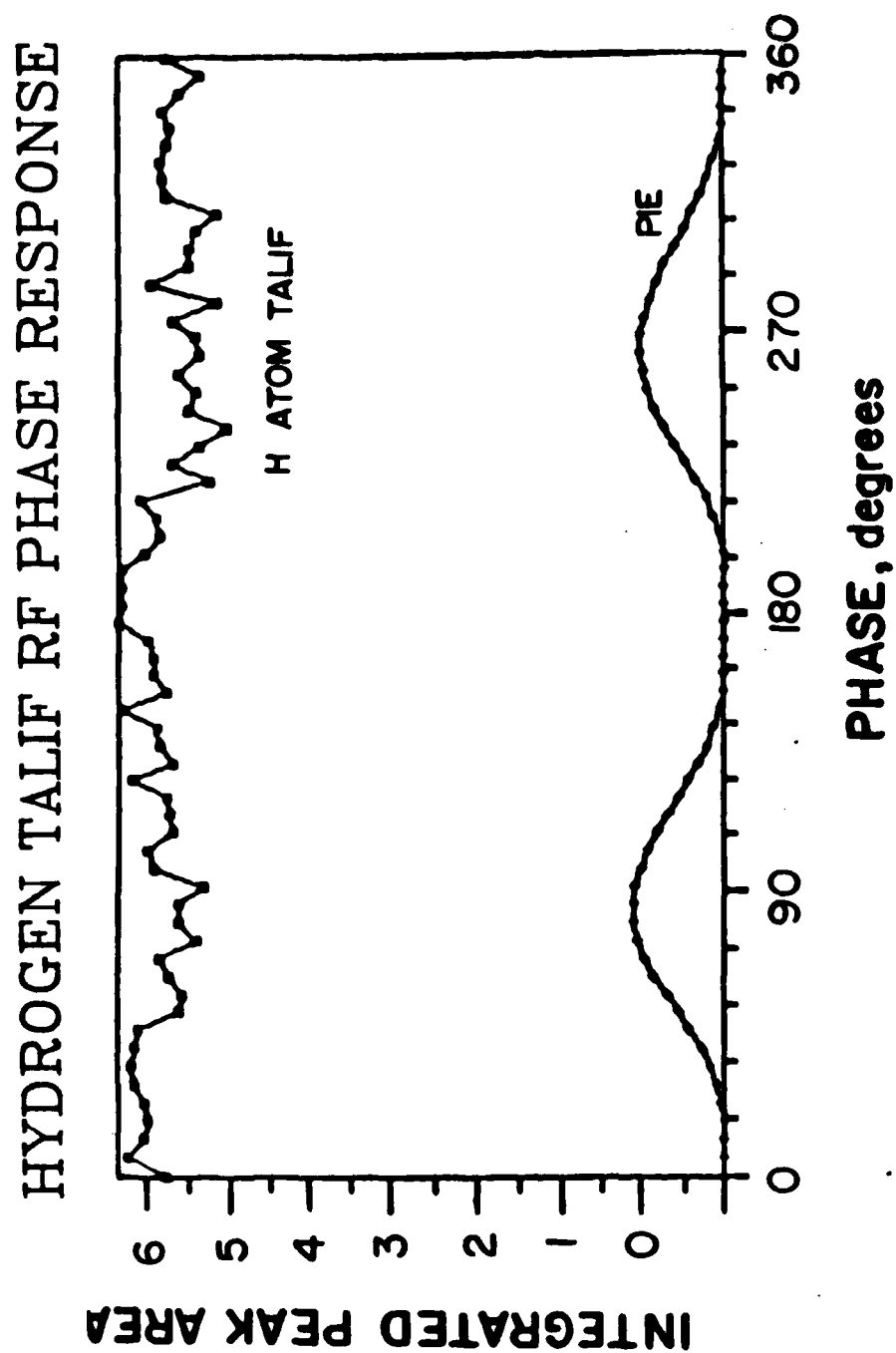


Figure 8. Ground-state H-atom concentration phase response. The upper trace is the TALIF signal and the lower trace shows the relative response of the PIE over a complete RF cycle.

TALIF SIGNAL CONCENTRATION DEPENDENCE

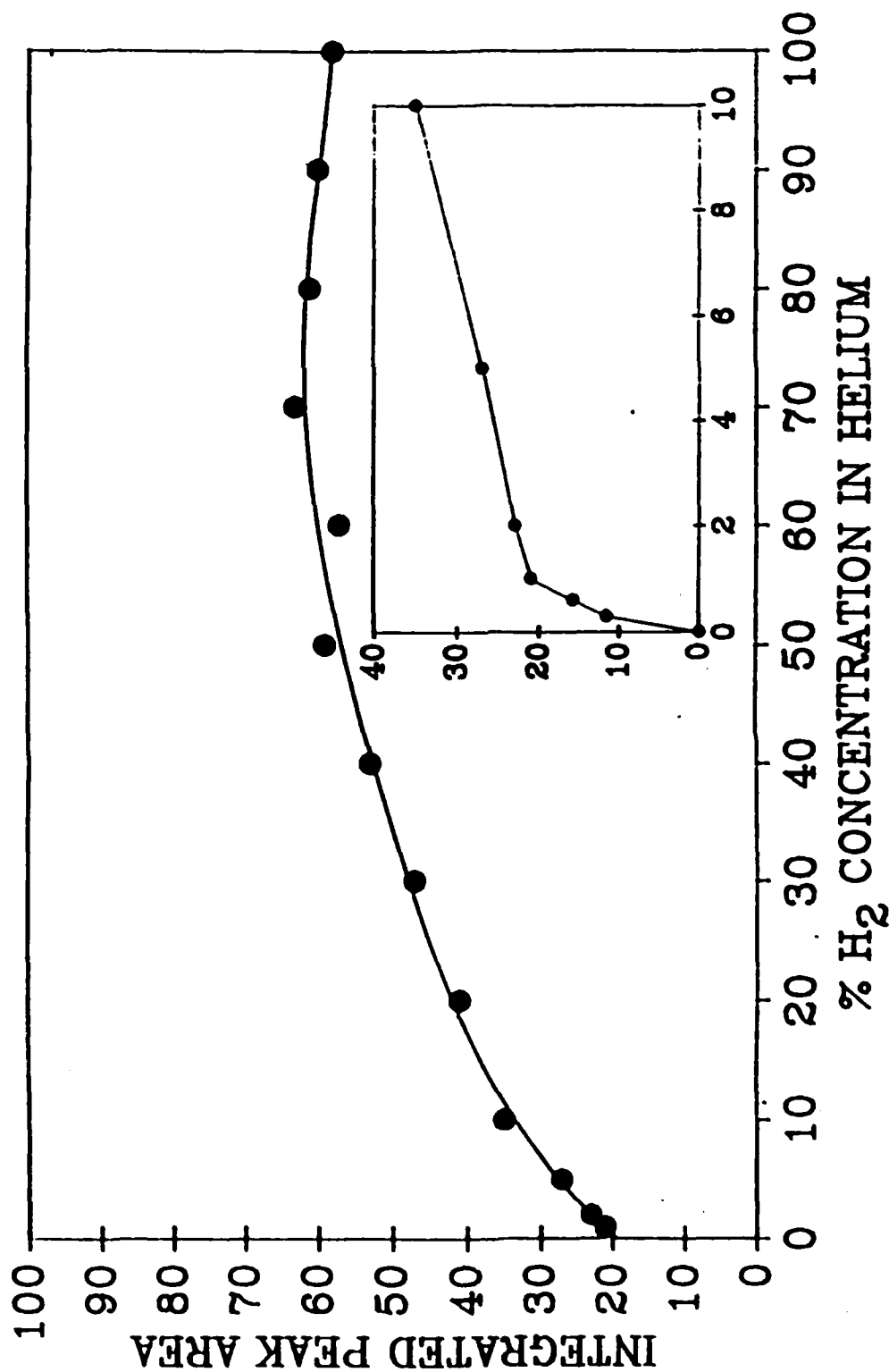


Figure 9. H-atom TALIF signal versus H₂ concentration in helium. The total discharge cell pressure is 1 Torr. The inset shows an expanded portion of the plot for concentrations below 10%.

shows that below ≈ 1 percent the TALIF response is nearly linear and passes through the origin.

B. H-ATOM PROFILES IN UNLOADED DISCHARGES

i) *Observations in continuous and pulsed discharges*

A typical axial profile of H-atom concentration at different positions across the interelectrode space of a continuous RF discharge and above the center of the electrode is shown in Fig. 10. It was taken with the laser frequency sitting at the peak of the transition while the translation stage is stepped to different positions across the 19-mm gap. All the spatial profiles shown in this work are corrected for the occultation of the detection solid angle from the electrode surface as the distance between the laser beam and the electrode surface gets smaller than 3.5 mm. A calculation of the reduction of the solid angle from which we collect the 656-nm fluorescence is checked by experiment. We fill the reactor cell with C_2H_2 at a pressure of 50 mTorr and we detect H-atoms produced by photolysis of the acetylene molecule with 205-nm photons.⁹ Since the detection of H-atoms takes place immediately after their production, within a laser pulse duration (10 ns), the concentration is independent of the position of production anywhere in the interelectrode space. The reduction in the TALIF signal that we observed is a result of the viewing reduction of the solid angle as the laser beam approaches the electrode surface, which is determined by the detection/collection geometry. We have found that the experimental determination of the geometrical view factor agrees within 10 percent with that calculated by geometrical considerations.¹⁰ As shown in Fig. 10, a concentration of about 8×10^{13} atoms/cm³ stays relatively constant over a wide region around the center of the discharge. As we approach the electrode surfaces, however, the concentration drops sharply to zero within 3-4 mm away from each electrode surface. We discuss below the

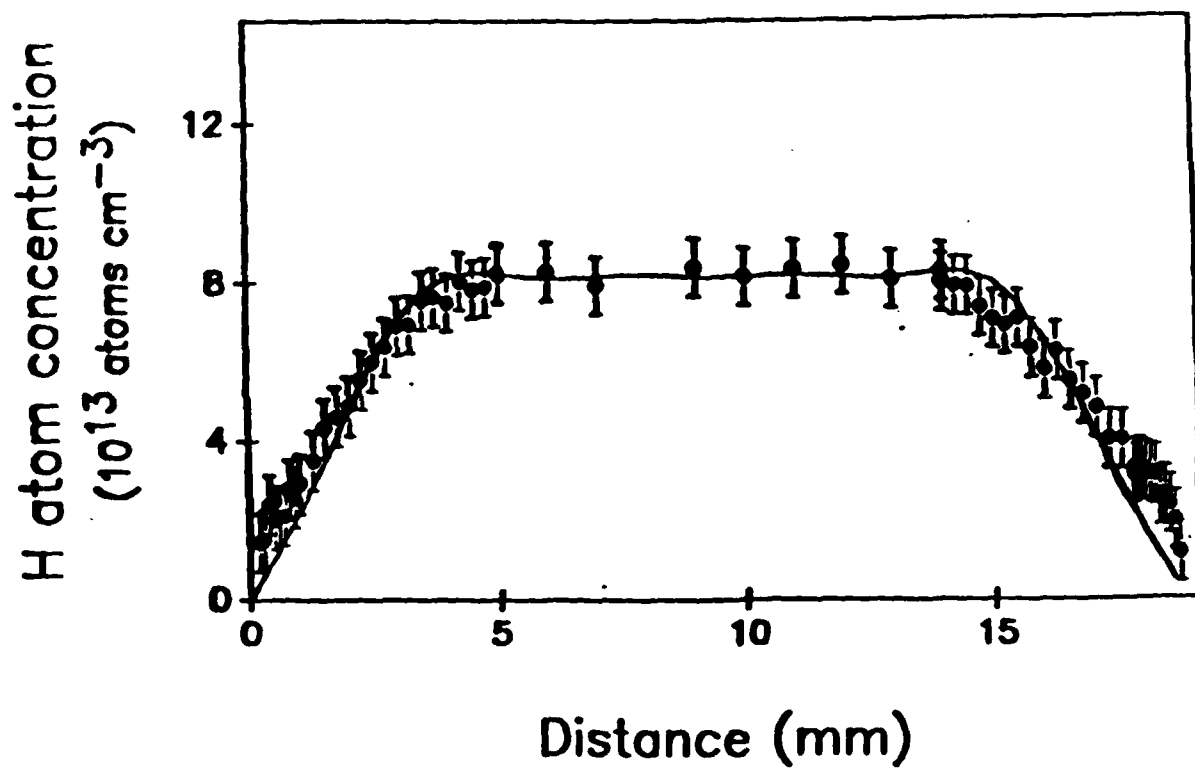


Figure 10. Typical H-atom concentration vs distance from the grounded electrode in a 10-MHz continuous discharge. The pressure of pure H_2 was 3 Torr and the power was 10 W. The ground and powered electrode positions are 0 and 19 mm. The solid line represents a fit obtained from the model discussed in the text.

mechanism that accounts for the observed concentration characteristics, where we model the temporal evolution of the concentration profiles. The solid line in Fig. 10 results from the proposed model (see 3.B.2) and shows a reasonably good agreement with the measurements.

Spatial profiles of hydrogen atoms are also taken in a pulsed discharge at different times after the discharge is turned on. In Fig. 11, we show the spatial distribution of H-atoms at 0.25 ms, 1 ms, and 2.5 ms. The figure describes the temporal evolution of H-atoms. The profile at 0.25 ms clearly shows that H-atoms are generated at regions centered at about 3.4 mm away from each electrode surface. The 1.0- and 2.5-ms traces show how the steady-state distribution builds up. H-atoms exit the production regions and fill the interelectrode space until they approach the metallic electrode surfaces, where they stick or recombine. The profile at 2.5 ms closely resembles that shown in Fig. 10, taken in a continuous RF discharge, indicating that a steady state is essentially established in the discharge at this point in time.

The profiles in Fig. 12 represent typical H-atom distributions after the discharge is turned off at t_0 . The spatial profiles shown are taken at elapsed time t after t_0 , with $t=0.25$ ms, $t=0.5$ ms and $t=1$ ms. It is clear that the electrodes represent a significant sink for H-atoms in the system. The solid lines shown in Figs. 11 and 12 represent best fitted theoretical concentration profiles which we discuss below.

Fig. 13 shows a temporal profile of the hydrogen atom concentration at the center of the discharge. The discharge is turned off at $t_0=2$ ms, a time close to the establishment of an equilibrium concentration in the discharge. The decay of hydrogen atoms follows a single exponential law as indicated by the linearity of the logarithmic fit displayed also in Fig. 13, that is independent of the atomic concentration at the time the discharge was turned off. The

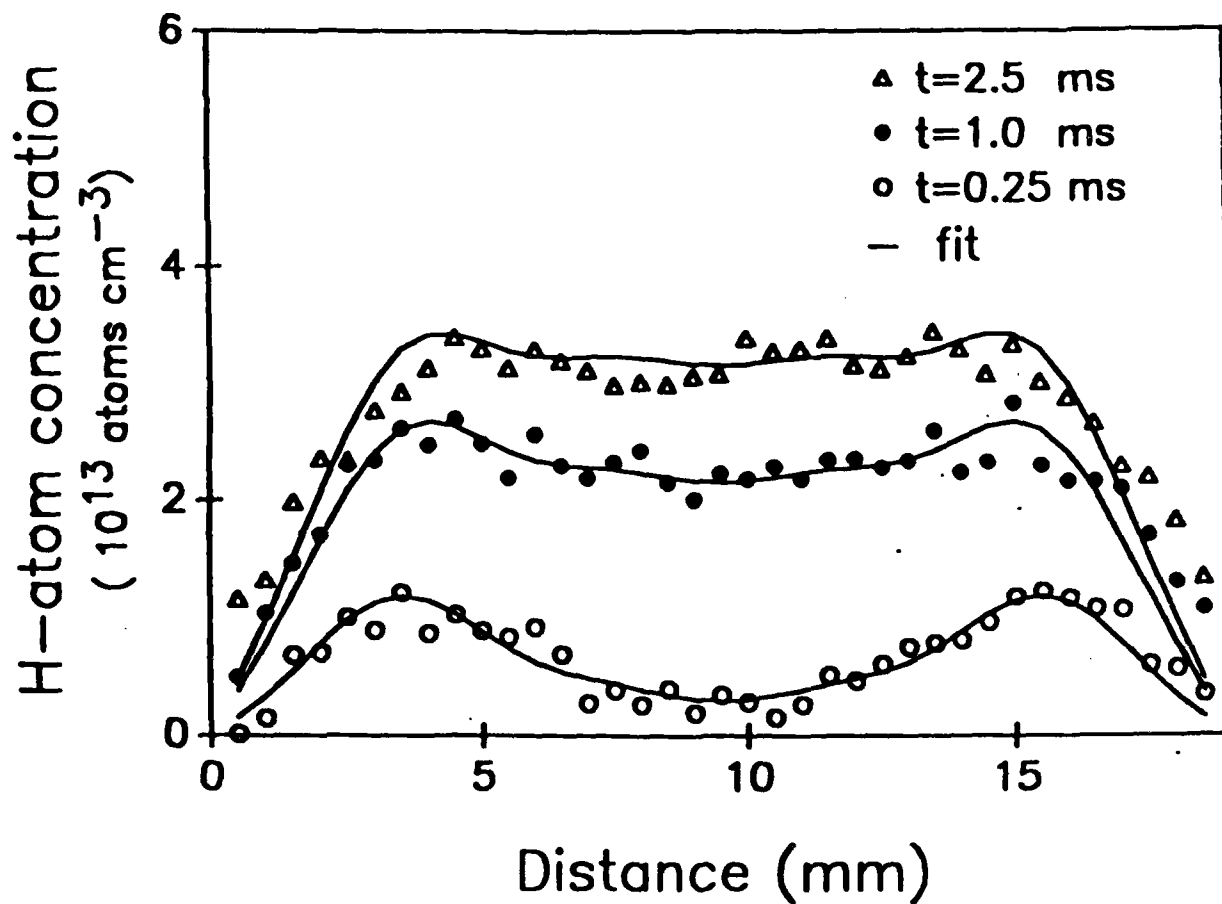


Figure 11. Temporal evolution of H-atom spatial profiles in a pulsed discharge; experimental data points and simulated results (solid lines) at $t=0.25$, 1.0 , and 2.5 ms . The pressure was maintained at 3 Torr and the power was 5 W.

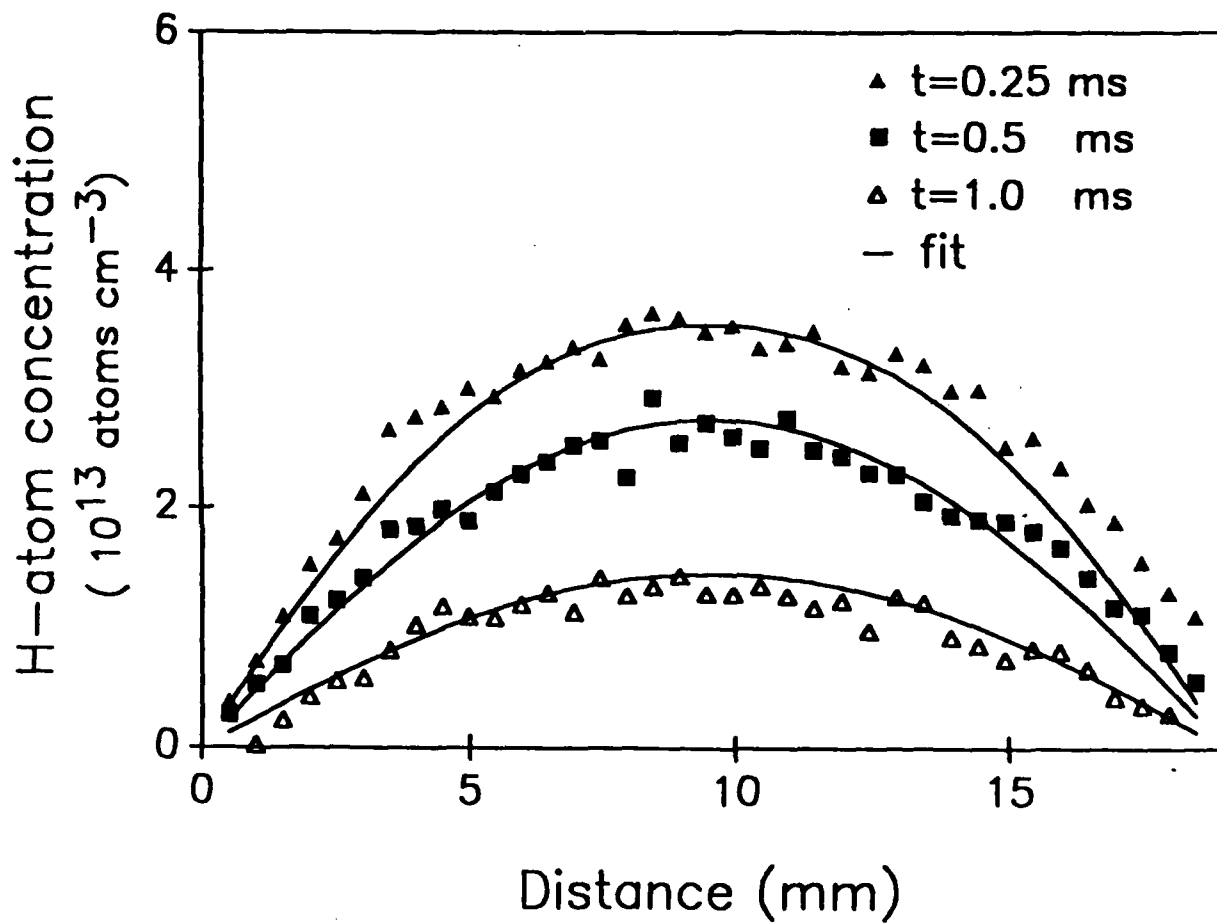


Figure 12. Decay of H-atom spatial distribution after switching the discharge off; experimental data points and simulated results (solid lines) at elapsed time $t = 0.25, 0.5$, and 1.0 ms after the discharge is turned off. Discharge conditions the same as in Fig. 11.

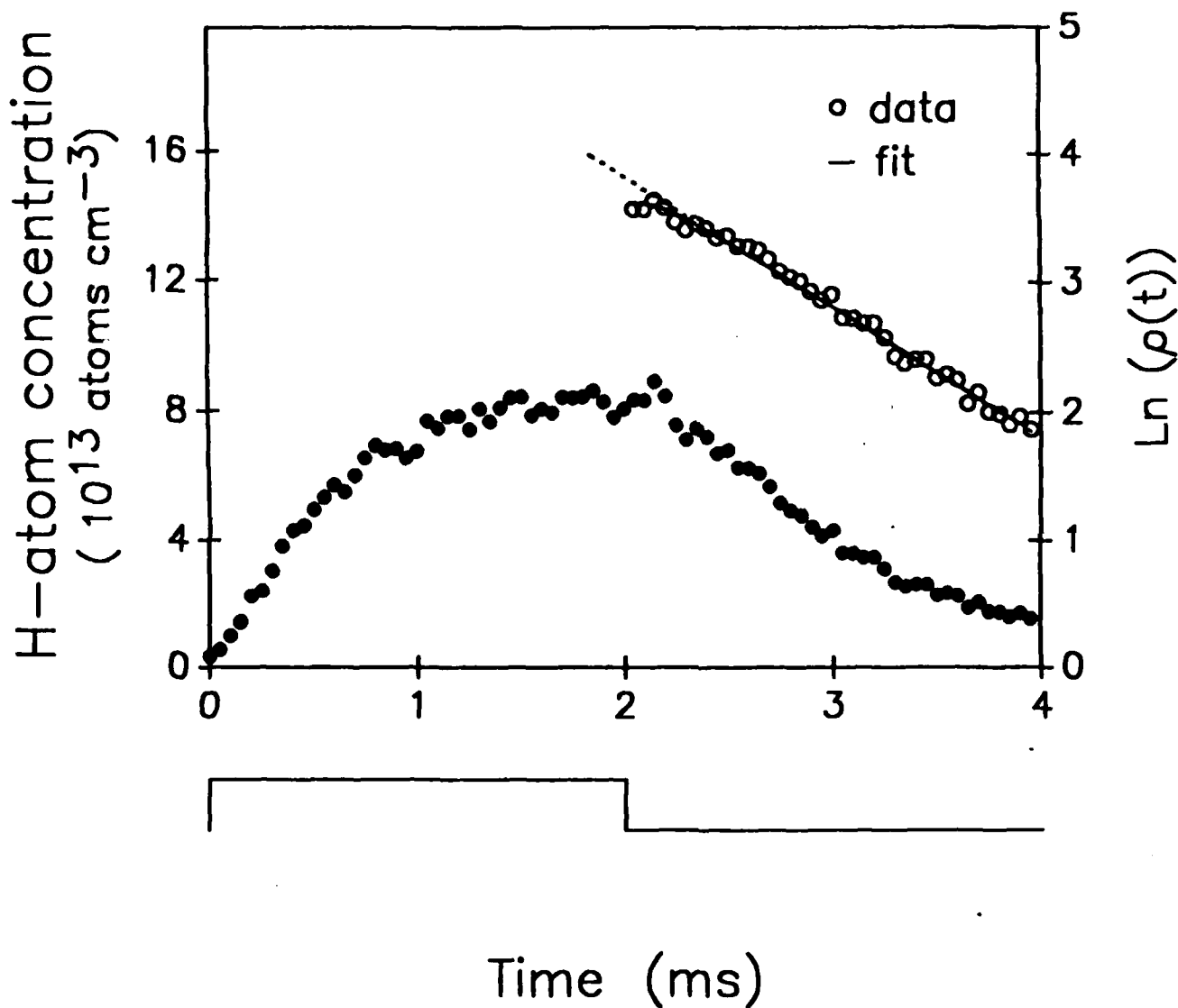


Figure 13. Temporal profile of H-atom concentration taken in the afterglow of a 2-ms pulse discharge at the center of the interelectrode space. A single exponential (as shown by log plot) can fit well the decay of H-concentration at times $\geq 200 \mu\text{s}$ after the discharge pulse ends. Discharge conditions as in Fig. 10.

exponential decay reveals that *first order* kinetics are responsible for the decay of hydrogen atom concentration after the discharge is turned off, with a time constant $\tau=1.03\pm0.08$ ms. Therefore, *gas phase* recombination of the hydrogen atoms is not significant since it would result in *second order* kinetics with respect to H-atom concentration.

Finally, we replace deuterium for hydrogen to check for any quantitative differences in behavior due to their mass difference. From the decay of the atomic deuterium concentration, we determine a time constant $\tau=1.66\pm0.10$ ms. The comparison of the time constants of hydrogen and deuterium indicates an approximate $m^{-1/2}$ dependence on the mass of the decaying particles.

ii) *Model*

The experimental observations presented in the previous section guided us in the formulation of a model that incorporates the following assumptions: First, the *gas phase* recombination is negligible as indicated by the simple exponential decay of the atomic hydrogen population. Second, the H-atoms are destroyed only on the metallic electrode surfaces which induce catalytical recombination and therefore represent sinks for H-atoms. Third, *neutral* diffusion governs the movement of the H-atoms towards regions of reduced atomic concentration in both the discharge and the afterglow. Finally, the production of H-atoms takes place in narrow regions in the discharge. These regions roughly coincide with the visibly brightest portion of the plasma, indicative of regions of high excitation and dissociation.

A quantitative formulation of our model is given as follows. Let x be the coordinate on the axis perpendicular to the electrode surfaces (see Fig. 1). Because of the symmetry of our discharge, we assume a uniform spatial distribution in y - and z - directions, so that the

atomic hydrogen concentration ρ depends only on x and t . We approximate the source regions with delta functions centered at a distance x_0 away from each electrode surface. Clearly, this assumption is oversimplified but, as we shall see, it yields reasonable results. Thus, we solve the one-dimensional diffusion equation:¹¹

$$\partial \rho / \partial t - D \partial^2 \rho / \partial x^2 = \rho_0 (\delta(x-x_0) + \delta(x-a+x_0)) \quad (4)$$

where D is the diffusion coefficient for the atomic species, ρ_0 is the production rate of the sources and a is the interelectrode separation. We will assume for simplicity that the electrodes are *perfectly* absorbing walls for the hydrogen atoms, and we impose the boundary conditions:

$$\rho(0,t) = \rho(a,t) = 0 \quad (5)$$

The validity of this assumption will be determined by the success of our fit. The solution expanded in a Fourier series is of the form¹²:

$$\rho(x,t) = \sum \rho_n(t) \sin(n\pi x/a) \quad n=1,3,5,\dots \quad (6)$$

where

$$\rho_n(t) = [4a\rho_0/(n^2\pi^2D)] \sin(n\pi x_0/a) (1-\exp(-D(n\pi/a)^2t)) \quad (7)$$

The solution of the diffusion equation after the discharge is turned off is given by Eq. (8):

$$\rho(x, t-t_0) = \sum \rho_n(t_0) \sin(n\pi x/a) \exp(-D(n\pi/a)^2(t-t_0)) \quad n=1,3,5,\dots \quad (8)$$

where t_0 is the time the discharge is turned off, and $\rho_n(t_0)$ is given by Eq. (7). The solid line shown in Fig. 13 represents a semilogarithmic fit of solution (8). Its linearity indicates that the first term of the expansion of the solution (8) is the dominant one in the decay of the atomic hydrogen concentration at the center of the discharge. The dashed line which resulted from a similar fit of the first only term of the expansion is indicative of the fact that higher order terms are important only for times $\leq 200 \mu\text{s}$ while they contribute less than 5 percent in the decaying concentration at times $\geq 200 \mu\text{s}$ after the discharge is turned off. The first term of the series relates the time constant τ of the exponentially decaying H-concentration to the diffusion coefficient D : $\tau=(a/\pi)^2/D$. We thus calculate the diffusion coefficients for H- and D-atoms to be $355 \pm 30 \text{ cm}^2/\text{s}$ and $220 \pm 15 \text{ cm}^2/\text{s}$ respectively. Actually, the comparison of the diffusion coefficients of these atoms provides a test for the model discussed above, since the diffusion coefficient depends inversely on the square root of the mass of the diffusing particle. The estimated values essentially agree with the expected $2^{1/2}$ ratio within the experimental uncertainty.

The steady-state spatial distribution $\rho_{ss}(x)$ is given by Eqs. (6) and (7), if we let $t \rightarrow \infty$:

$$\rho_{ss}(x) = 4a\rho_0/(\pi^2 D) \sum (1/n^2) \sin(n\pi x_0/a) \sin(n\pi x/a) \quad n=1,3,5,\dots \quad (9)$$

We fit the theoretical spatial distribution to the experimental data with parameters D , ρ_0 , and x_0 . The best fitting curves obtained by a least square fit program are shown (along with the

data used for the fits) in Figs. 10, 11, and 12. We estimate the position of the sources to be at 3.4 ± 0.2 mm away from the electrode surfaces, the production rate ρ_0 to be $(4.1 \pm 0.6) \times 10^{16}$ atoms/cm²sec and 7.8×10^{16} atoms/cm²sec in the pulsed and the CW discharge respectively (operated at 5 W and 10 W). The value of the diffusion coefficient D as determined in these spatial profile fits is 380 ± 60 cm²/s. This value agrees well with the value from the temporal decay data and agrees (within the uncertainty) with that of 440 cm²/s as calculated from Gilliland's semiempirical equation.¹¹ This equation based on kinetic theory assumes a $T^{3/2}$ dependence for the diffusion coefficient and it is evaluated at 300 K (we assume thermally equilibrated H-atoms at room temperature). The production of energetic species at regions located several millimeters away from the surfaces, has been indicated previously for species such as F* metastables,¹³ O atoms,¹⁴ and BCl radicals¹⁵ at high frequencies. It was shown in the last work that the production of radicals is affected by the frequency of the discharge. One may also expect that the pressure affects the regions of production of energetic species. Therefore the dependence of the location of the H-atom sources on frequency and pressure should be the subject of further study.

The best fitting line we show in Fig. 10 represents the steady-state spatial solution (9) for totally absorbing surfaces at $x=0$, $x=a$. However, the experimental concentration gradient near the electrode surfaces is smaller than that calculated from Eq. (9), an indication that the electrode surfaces are *partially* absorbing with a loss coefficient γ_s for H-atoms:

$$\gamma_s = D(\partial \rho / \partial x) / [D(\partial \rho / \partial x) + v \rho / 4] \big|_{x \rightarrow 0}, \quad (10)$$

where $D(\partial p/\partial x)|_{x \rightarrow 0}$ is the flux of H-atoms that are absorbed on the stainless steel electrode surface at $x=0$ and $v\rho/4$ is the flux of H-atoms of mean thermal velocity v striking on the surface without sticking. The loss coefficient of H-atoms on a surface can be determined from semilogarithmic fits of the steady state spatial profiles near the electrode surfaces, as those shown in Fig. 14. The fitting curves are obtained by solving the diffusion equation for boundary surfaces with a loss coefficient $\gamma_s=5$ percent for hydrogen and deuterium atoms. The uncertainty in determining γ_s from the semilogarithmic fits is ± 1 percent. The loss coefficients for hydrogen and deuterium are equal, as one would expect from expression (10) for γ_s since the mean thermal velocity and the diffusion coefficient both vary as $m^{-1/2}$. The result further verifies the fact that the balance between diffusion and atom removal at the surface establishes the observed concentration gradient close to the electrode surfaces. In addition, the value $D=355 \pm 20$ cm²/s determined by the temporal decay should then be modified to account for the *partially* absorbing electrode surface. Numerical solution of the diffusion equation for H-atoms confined between two surfaces with a 5 percent loss coefficient gives a corrected value of $D=460 \pm 25$ cm²/s, in close agreement with the literature value $D=440$ cm²/s.

C. H-ATOM PROFILES IN LOADED DISCHARGES

i) *Experimental observations*

In Fig. 15, we show hydrogen atom concentration profiles taken 1.5 mm above the grounded bottom electrode while the reactor cell is translated horizontally (radial profiles). The radial profile shown in Fig. 15(a) is taken over a 10x10 mm GaAs wafer. We observe a significant increase in hydrogen atom concentration localized over the wafer surface. A radial profile over an identical stainless steel piece, shown in Fig. 15(b), proves that the drastic

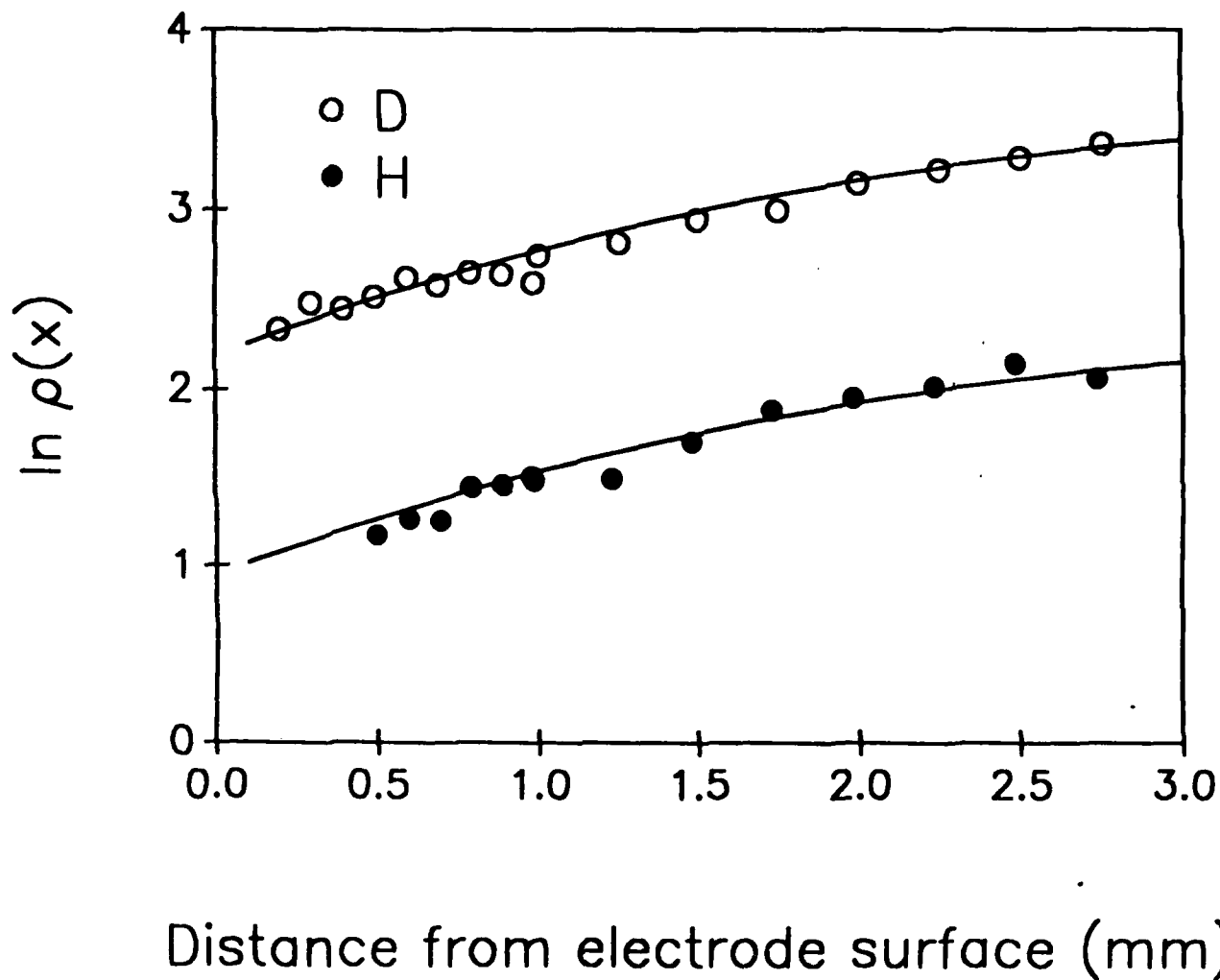


Figure 14. Steady-state concentrations for H- and D-atoms at small distances from the stainless steel electrode surface. The solid lines are fits obtained for surfaces with a loss coefficient $\gamma_i = 5\%$ for hydrogen and deuterium atoms. Discharge conditions the same as in Fig. 10.

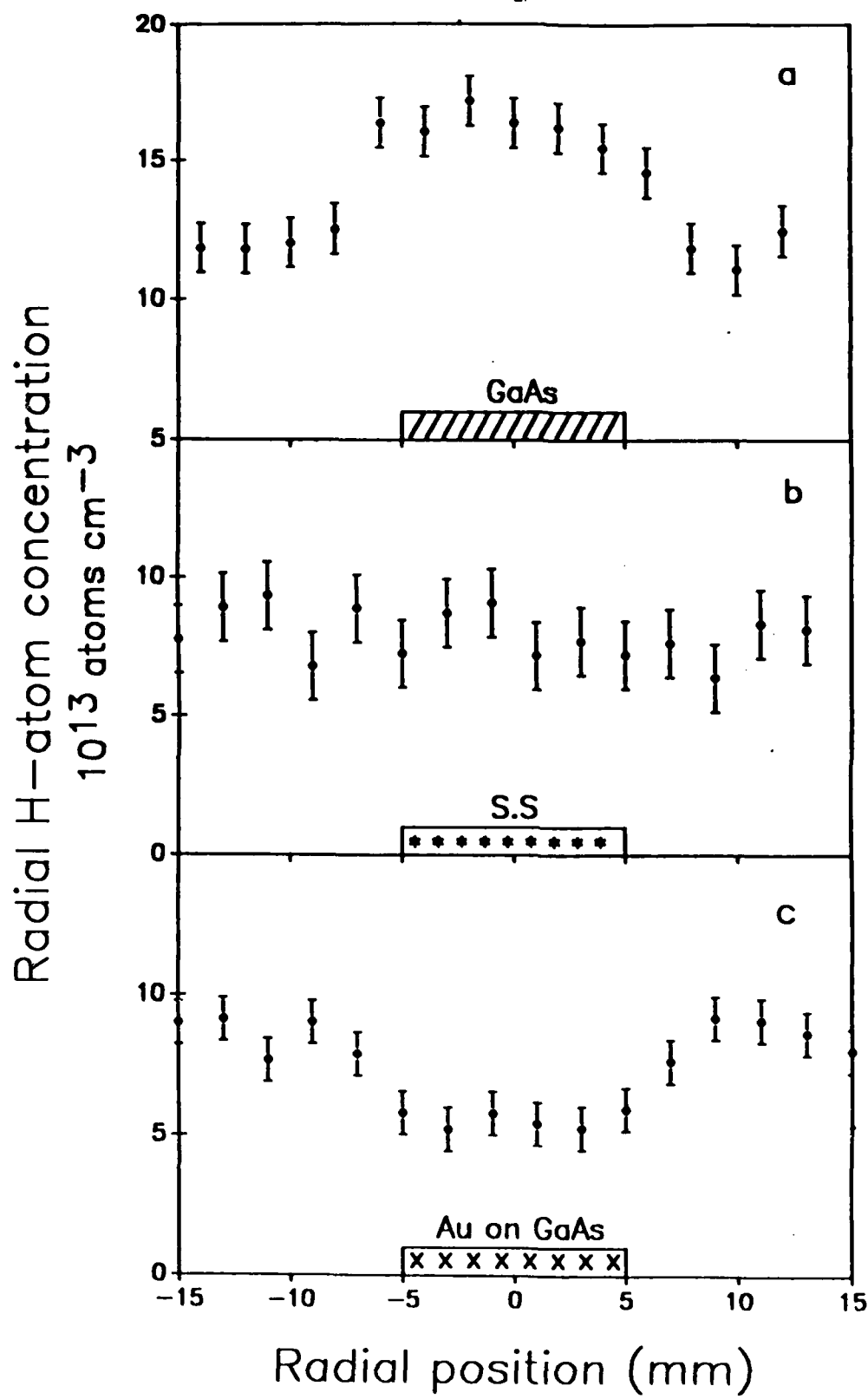


Figure 15. Comparison of radial profiles of H-atom concentration probed 1 mm above (a) a GaAs wafer, (b) a stainless-steel substrate, and (c) a gold coated GaAs wafer. Al wafers of $10 \times 10 \times 0.5$ mm size are centered on the stainless-steel ground electrode extending from -25 mm to +25 mm of the x-axis.

change in the concentration cannot be attributed to changes in the bulk properties of the discharge, or in the detection geometry. The GaAs surface must be responsible for the increase in the concentration, as we further verified by depositing 2- μm -thick gold on the GaAs. A radial profile taken over the gold coated GaAs wafer, shown in Fig. 15(c), indicates a *reduction* in the hydrogen concentration and suggests that a surface/atomic hydrogen interaction must be occurring.

By employing a *pulsed* discharge, we studied the temporal development of the hydrogen concentrations in the interelectrode space. In Fig. 16 we show hydrogen atom concentrations in a discharge loaded with a 15-cm² GaAs wafer at various times after the onset of the discharge. Specifically, the spatial concentrations shown were measured at times $t=0.15$ ms, 0.50 ms, and 2.50 ms. The profile at $t=0.15$ ms indicates that the production of hydrogen atoms in these plasmas occurs in localized regions in close proximity to the electrodes. In time the hydrogen atoms diffuse from their sources towards the center and the electrode surfaces. We observe that the spatial profile at very early times is not affected by the presence of the GaAs wafer; however, as time increases, the concentration of the hydrogen atoms builds up close to the wafer surface, resulting to the apparent spatial asymmetry of the profile taken at time $t=2.5$ ms.

In Fig. 17, we show axial profiles of hydrogen atom concentration in a *continuous* discharge, unloaded and loaded with Si and GaAs wafers. A typical axial profile in a continuous unloaded hydrogen discharge is shown in Fig. 17(a). A concentration of 8×10^{13} atoms/cm³ stays relatively constant over a wide region in the interelectrode space, until it exhibits a considerable gradient in the regions 0-4 mm away from each electrode surface. In

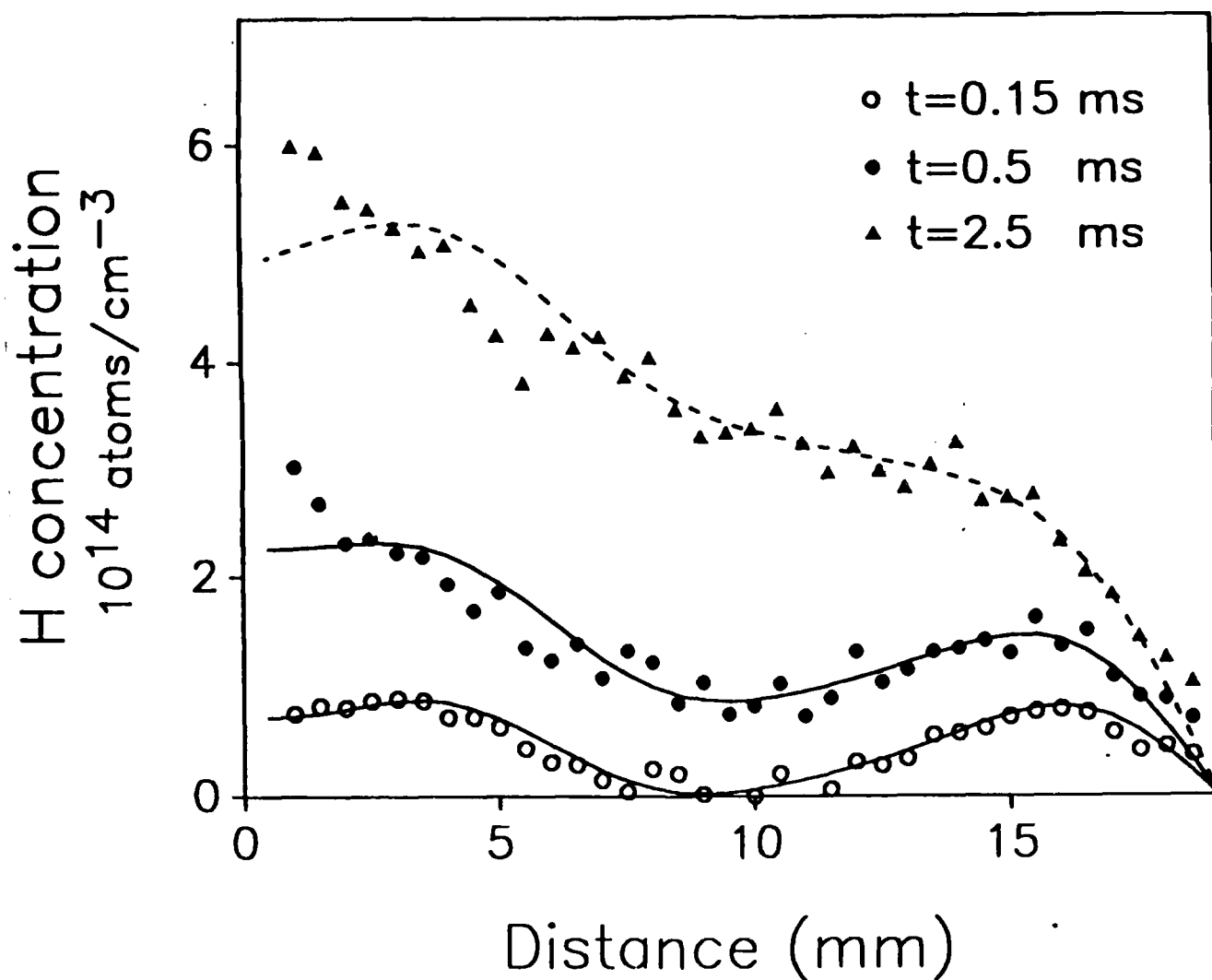


Figure 16. Evolution of H-atom spatial distribution in a pulsed discharge loaded with a GaAs wafer on the grounded electrode; experimental data points and simulated results (solid and dashed lines) at $t=0.15$ ms, $t=0.50$ ms, and $t=2.50$ ms. The location of the ground and powered electrodes is a 0 and 19 mm, respectively. Discharge conditions: pressure of 3 Torr, and power of 40 W.

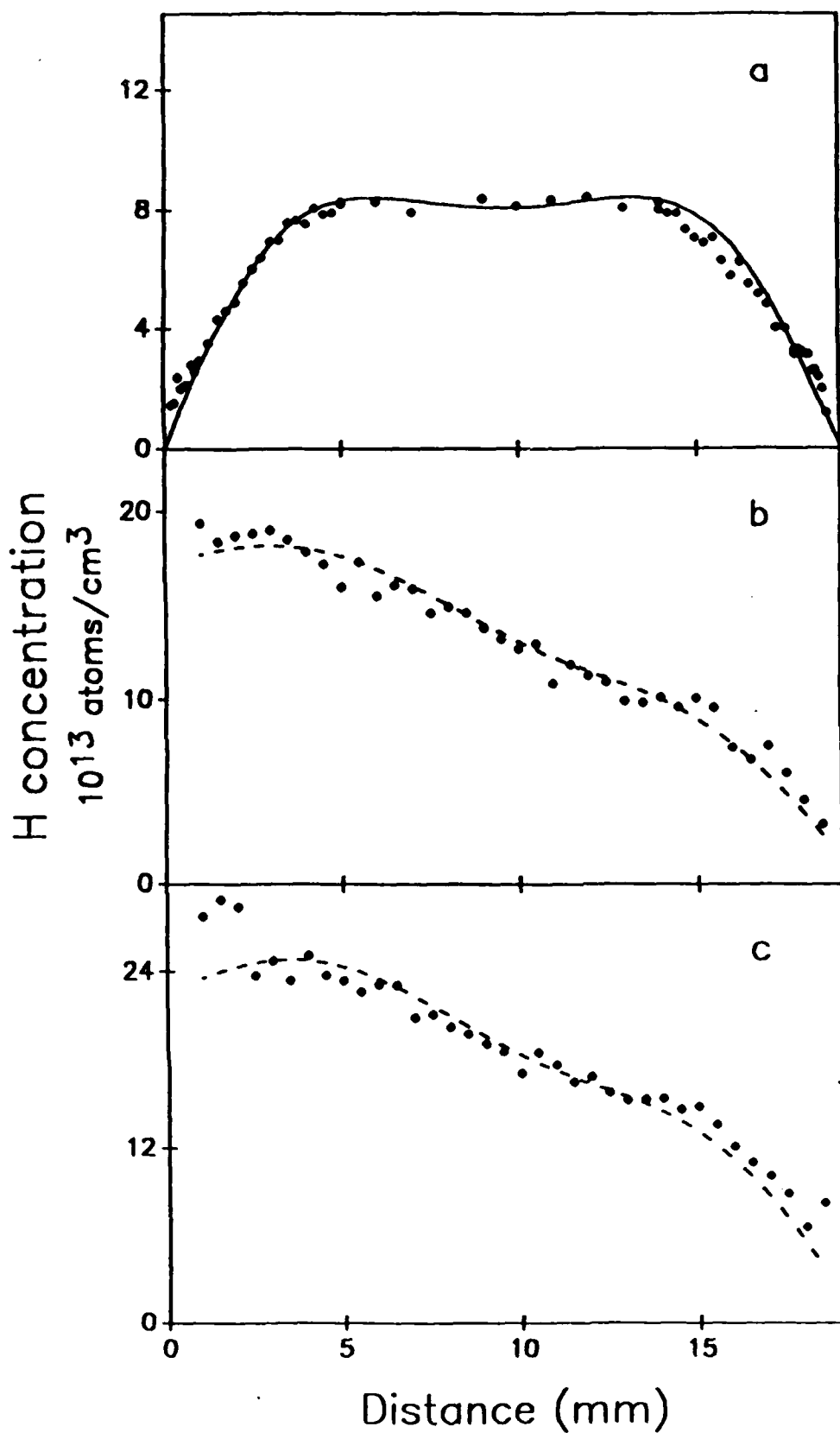


Figure 17. H-atom concentration vs. distance from the grounded electrode in a continuous discharge: (a) unloaded, loaded with (b) a Si wafer, and (c) a GaAs wafer placed on the grounded electrode (0-0.5 mm). The solid and dashed lines represent fits obtained from a diffusion model. Discharge conditions: pressure of 3 Torr, and power of 10 W.

Fig. 17(b) we show an axial profile taken under identical conditions with the exception that a Si wafer is placed on the grounded electrode, covering three-fourths of the electrode surface area. We observe a significant qualitative difference from the previous profile. The hydrogen concentration appears considerably increased in the region from the center of the discharge to the electrode surface that bears the Si wafer. Similarly, Fig. 17(c) shows a spatially asymmetric hydrogen profile in a discharge loaded with a GaAs wafer.

ii) *Model*

We explain the observed behavior of the H-concentration with an extension of the model for an unloaded discharge, according to which these profiles are determined by diffusion of the hydrogen atoms from the regions where they are produced towards the surfaces which confine the plasma. The model assumes *two point sources* of hydrogen atoms located at a distance x_0 away from each electrode surface. We also assume that what differentiates the behavior of the atomic concentration at the presence of different surfaces in the discharge is the nature of the surfaces themselves. Metallic surfaces are known to enhance the heterogeneous reactivity of radicals as opposed to oxidized semiconducting surfaces.¹⁶ Direct evidence for that is provided in Fig. 15, where H-atoms are consumed near metallic surfaces (stainless steel and gold) rather than near the GaAs surface. Consequently, we assume in a first approximation that the stainless steel electrodes represent a perfectly absorbing surface for the hydrogen atoms with a sticking or recombination coefficient close to 1, while the semiconducting surfaces represent totally reflecting surfaces. We again solve the diffusion equation¹¹ for the hydrogen atom density $\rho(x,t)$:

$$\partial \rho / \partial t - D \partial^2 \rho / \partial x^2 = \rho_0 (\delta(x-x_0) + \delta(x-a+x_0)) \quad (11)$$

where ρ_0 is the production rate of the H-atoms, D is the diffusion coefficient for H-atoms, x_0 is the distance of the point sources from each electrode, and a is the interelectrode distance. For the unloaded discharge the boundary conditions were $\rho(0,t)=\rho(a,t)=0$. Above a wafer loaded on the electrode at $x=0$, we set the boundary conditions $\partial \rho / \partial t(0,t)=0$, $\rho(a,t)=0$. Then the solution of Eq. (11) is:

$$\rho(x,t) = 2a\rho_0/(\pi^2 D) \sum \rho_n(x) [1 - \exp(-(n+1/2)^2(\pi/a)^2 Dt)] \quad n=0,1,2,\dots \quad (12)$$

where

$$\rho_n(x) = (n+1/2)^{-2} [\sin((n+1/2)\pi x_0/a) + (-1)^n \cos((n+1/2)\pi x_0/a)] \sin((n+1/2)\pi(a-x)/a) \quad (13)$$

We discuss the validity of this model in describing the data in Figs. 16 and 17. The solid lines in Fig 16 represent the solutions (12) of the diffusion equation at $t=0.15$ ms and $t=0.50$ ms. For both fits the diffusion coefficient is $390 \text{ cm}^2/\text{s}$, the H-atom sources are centered at 3.4 mm away from each electrode surface, and the production rate of the hydrogen atoms is $3.2 \times 10^{17} \text{ atoms/cm}^2\text{s}$. The values of the parameters $D=390 \pm 60 \text{ cm}^2/\text{s}$ and $x_0=3.4 \pm 0.2 \text{ mm}$ were also used to successfully fit the steady-state concentration profile in an unloaded discharge (see Fig. 17(a)), as well as temporally evolving spatial profiles of atomic hydrogen in unloaded discharges.¹⁷ The value of the diffusion coefficient D for the hydrogen atoms is in agreement (within the uncertainty) with the value of $440 \text{ cm}^2/\text{s}$ which has been calculated assuming a $T^{3/2}$

dependence of D .¹¹ The fact that we obtain reasonably good fits for loaded and unloaded discharges with the same value of x_0 leads to the conclusion that the presence of the semiconducting surfaces does not alter the location of the sources of hydrogen atoms, at least as far as the sensitivity of our method allows us to measure.

The experimental data at $t=2.50$ ms show a hydrogen atom concentration substantially lower than what the model predicts for a *perfectly* reflecting surface. A *partially* reflecting GaAs surface may accommodate this discrepancy. The dashed line shown in Fig. 16 represents a fit which uses the H-concentration just above the GaAs surface as a parameter. We found that a reduction of the hydrogen atom concentration adjacent to the GaAs surface by about 30 percent of its value near a perfectly reflecting surface or equivalently a 0.2 percent sticking or recombination coefficient for the GaAs surface provides a reasonably good fit to the data. This result represents a recombination coefficient typical for native oxides¹⁸ inherent on the semiconducting surfaces.

The solid line in Fig. 17(a) represents the solution (3) of the diffusion Eq. (2) at steady state ($t \rightarrow \infty$). The parameters for the fit are $D=390 \pm 60$ cm²/s, $x_0=3.4 \pm 0.2$ mm and $\rho_0=7.8 \times 10^{16}$ atoms/cm²s. The production rate ρ_0 is lower than that in the pulsed discharge due to the smaller power we used for the continuous discharge (10 W) as opposed to a power of 40 W for the pulsed discharge. We observe that the model is in good agreement with the data for the unloaded discharge. To fit the data taken in the loaded discharges (Figs. 17(b), 17(c)), we had to use the H-concentration adjacent to the Si and GaAs surfaces as a parameter, as we did for the fit in Fig. 16(c). The dashed lines in Figs. 17(b), 17(c) represent fits with the same parameters D , x_0 and a decrease of the concentration of H-atoms adjacent to the Si and GaAs

surfaces by about 40 percent. The agreement between the simulations and the experimental data is indicative of *partially* reflecting surfaces or equivalently a partial loss of atomic H on the surface. The consumption of H-atoms may further rise by the removal of native oxides inherent on the surfaces in discharges at lower pressures containing heavier etchant gases.^{19,20} Clearly, further investigation is required to illuminate the details of the interaction between the hydrogen atoms and the semiconducting surfaces.

D. LINEWIDTHS AS A PROBE OF DISCHARGE TEMPERATURE AND PURITY

This study focussed on determining the temperature of H-atoms in the RF discharge. The kinetic energy of reactive species in a plasma should be a key parameter in the modeling of reactor phenomena and may have significant effect on devices or materials produced by the processing.

Assuming the H-atoms are produced by the discharge itself, conventional wisdom suggests that such a relatively long-lived species will be equilibrated with the overall heavy particle temperature. However, previous work²¹ utilizing plasma induced emission has determined that a large fraction of the H-atoms in excited electronic states are very hot indeed, with temperatures in excess of 10^6 K. The present experiments provide the first comparable measurement for ground state H-atoms, obviously the numerically predominant form present in the plasma.

In the emission work, the mechanism heating the excited state atoms is charge exchange with fast moving (hot) hydrogen ions, H^+ , H_2^+ , H_3^+ , accelerated by the electric fields in the discharge. A similar ion exchange mechanism almost certainly exists for ground state H-atoms. The question is whether their somewhat longer lifetime is sufficient to equilibrate the vast

majority of them to ambient temperature.

Another mechanism that will produce hot H-atoms is H_2 electron impact dissociation process in the plasma which is well known^{22,23,24,25} to produce atoms with translational energies of order 10^4 K. Again, the question is whether these hot atoms are equilibrated to ambient temperature.

A final process which can produce hot H-atoms is the TALIF diagnostic itself. Photodissociation of a molecule, like electron impact dissociation, can produce very hot atoms. Since photodissociation cross sections of ground state H_2 by 205-nm photons are small, photodissociation by the diagnostic laser is a negligible process in a pure H_2 plasma. However, many hydrogen containing molecules, e.g. NH_3 , hydrocarbons from pump oil and elsewhere, etc., have bond energies less than that of the 205-nm diagnostic photons and appreciable cross sections. Should those molecules be present, either as feedstock gases, contaminants, or via plasma synthesis, then photodissociation leading to hot H-atoms is quite likely. Moreover, these H atoms will likely be detected before they have any opportunity to undergo equilibrating collisions, since they may be observed by subsequent 205-nm photons in the same laser pulse whose duration is ~ 5 nsec, shorter than the lifetimes of the hot excited state H-atoms previously observed to be produced by ion exchange. Thus H-atoms produced photolytically will bear a spectral profile signature characteristic of their precursor molecule.

During our work we have analyzed H-atom TALIF signals produced both in an RF H_2 plasma and downstream from an H_2 microwave plasma. We have also examined RF plasmas containing other processing gases such as ammonia, acetylene and hydrogen sulfide, and these results will be discussed.

i) *Theory*

Our procedure for determining H-atom temperatures is to measure the TALIF linewidth. Under ideal conditions, the experimental line profile will be entirely determined by Doppler broadening. In this case, the full width at half height, $\Delta\nu_D$, is related to the atomic velocity and temperature by²⁶

$$\Delta\nu_D = 2\nu_0(\bar{v}/c) = (2\nu_0/c) \left(\frac{2kT \ln 2}{m} \right)^{1/2} = 7.16 \times 10^{-7} (T/M)^{1/2} \nu_0 \quad (14)$$

where

\bar{v} = average velocity of the atom or molecule

c = speed of light

ν_0 = transition frequency

k = Boltzmann constant

m = mass of the atom or molecule

T = temperature of the atom or molecule

M = molecular weight in amu of the atom or molecule

To give one an appreciation of the magnitudes involved, it is useful to evaluate Eq.(14) for H-atoms at ambient temperature (300K). The experimentally assessed TALIF $3\ ^2S(^2D) \leftrightarrow 1\ ^2S$ H-atom transition occurs at $\nu_0 = 97492\text{ cm}^{-1}$. Thus $\Delta\nu_D = 1.21\text{ cm}^{-1}$ for ambient H-atoms. Considering the fact that we combine 6 dye laser photons to drive this transition implies that the maximum width of our dye laser should be $\leq 0.1\text{ cm}^{-1}$ to produce a predominantly Doppler broadened line. Additionally, we note that because the molecular weight occurs in the

denominator of Eq.(14), the requirement on the dye laser linewidth will be much more stringent to obtain temperatures of other reactive atoms.

ii) *H₂ Discharge*

To establish a reference for measuring ambient TALIF linewidths, microwave generated hydrogen atoms were detected after flowing down a few centimeters of tubing. The microwave discharge, well removed from the region of fluorescence capture, does not contribute the bright PIE present in the RF plasma cell; therefore, a continuous wave photomultiplier tube was used to initially record the H-atom resonance. This was a test to ensure that the response time of the gated tube did not bias our linewidth measurements. Using this configuration, a linewidth of $1.34 \pm 0.07 \text{ cm}^{-1}$ (fwhm) was measured for low laser powers ($< 30 \text{ } \mu\text{J}$). Treating the lineshape as Gaussian and deconvoluting a laser linewidth of 0.42 cm^{-1} (fwhm, 3 photons to produce 205-nm x 2-photon process; $6 \times 0.07 \text{ cm}^{-1}$) results in an inherent Doppler width of 1.27 cm^{-1} , which corresponds to a temperature from Eq.(14) of $330 \pm 35\text{K}$. Although this is slightly hotter than room temperature, it agrees within experimental uncertainty. A small contribution from laser saturation broadening may also add slightly to linewidth.

Linewidths measured with the GPMT under the same conditions were $1.47 \pm 0.08 \text{ cm}^{-1}$. This value was very sensitive to integration parameters, for example, gate width and gate position. A gatewidth of 75 ns and gate position centered on the resonance produced the narrowest measurements. The slight discrepancy between the CWPMT and the GPMT is attributed to the response of the gated tube. The GPMT has a tendency to easily saturate, giving the appearance of a slightly broadened line. The value of 1.47 cm^{-1} was taken to correspond to the ambient temperature inclusive of instrumental broadening for the GPMT.

The simple Gaussian deconvolution leads to an effective instrumental contribution of 0.6 cm^{-1} .

Determination of the temperature for the RF discharge H-atoms followed the same procedure used to record the narrowest H-atom signals produced from the microwave discharge. For low discharge powers and low discharge pressures ($\approx 0.5 \text{ torr}$, $< 12 \text{ W}$) a minimum linewidth of $1.64 \pm 0.2 \text{ cm}^{-1}$ is obtained, corresponding to a temperature of $440 \pm 140 \text{ K}$ after instrumental and laser linewidth contributions are considered. A representative H-atom spectrum is shown in Fig. 18.

The relatively large uncertainty in the temperature measurement in the RF discharge, caused by PIE and by using low laser powers to minimize saturation, can arguably equate the microwave and RF temperature; however, other evidence suggests that the RF environment is hotter than ambient under most conditions. When the rf power or the H_2 pressure is increased from the minimum, the linewidth and hence the temperature also increased to a maximum of over 1000 K (see Fig. 19). Deuterium data were also recorded and showed a linewidth $2^{1/2}$ times narrower than H-atoms, ensuring that the increase in width is related to Doppler broadening.

Data for microwave and RF discharge produced H-atoms were also recorded employing the dye laser without the intracavity etalon. These grating scans served primarily as survey data, but reflect the same trends for the pressure and RF power dependence on linewidth, when the much larger laser linewidth contribution is deconvoluted.

Such high temperatures for the H-atoms are somewhat surprising, especially considering that previous measurements for temperatures of BCl^{17} and O^8 atoms in RF plasmas are 300 K . One would expect that the neutral species should be equilibrated to the ambient temperature of the reactor walls.

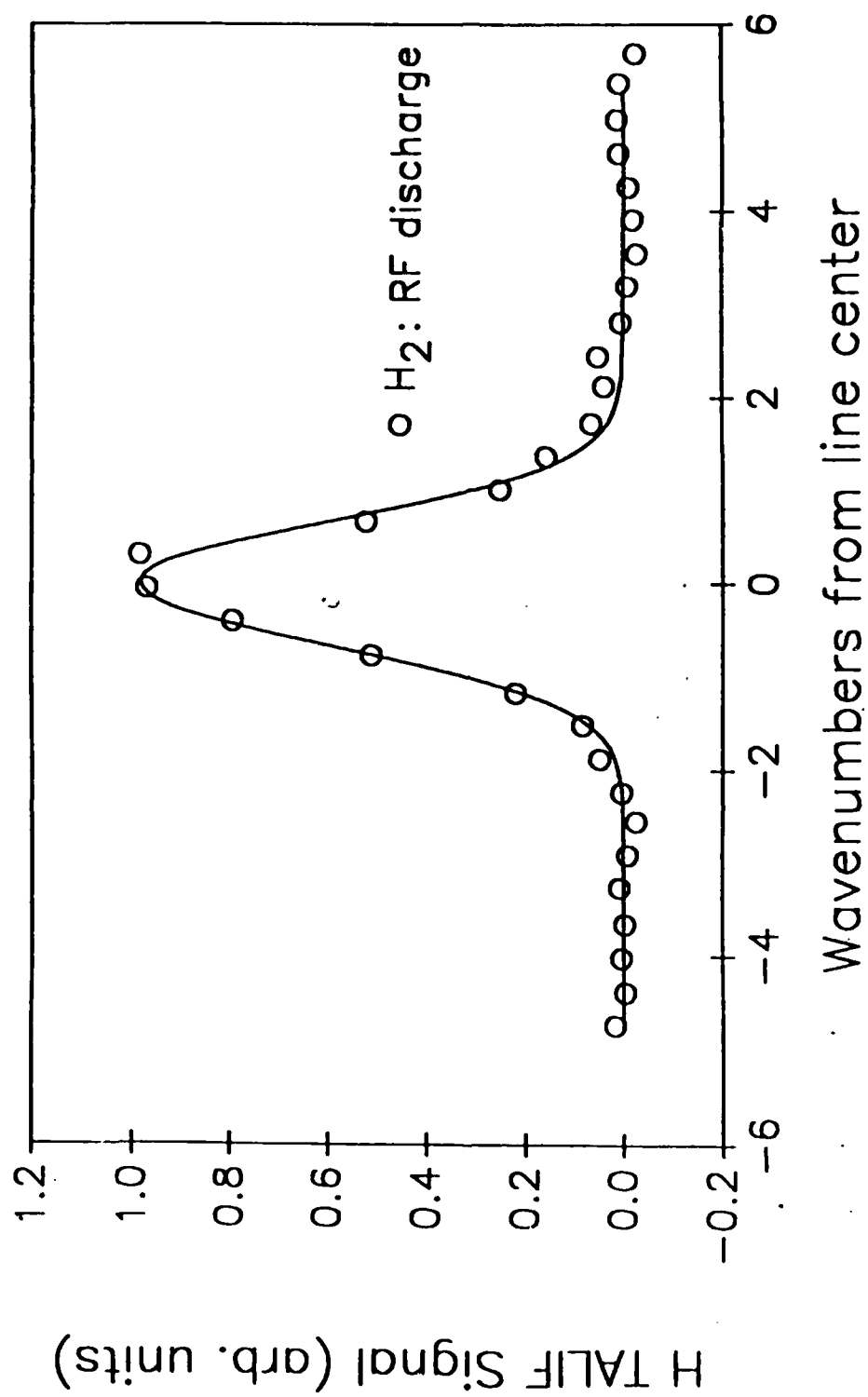


Figure 18. Etalon narrowed TALIF scan of the H atom $3^2S(D) \rightarrow 1^2S(97,492.3 \text{ cm}^{-1})$ transition from atoms generated in an RF discharge. Actual data points and a Gaussian fit to the data are presented.

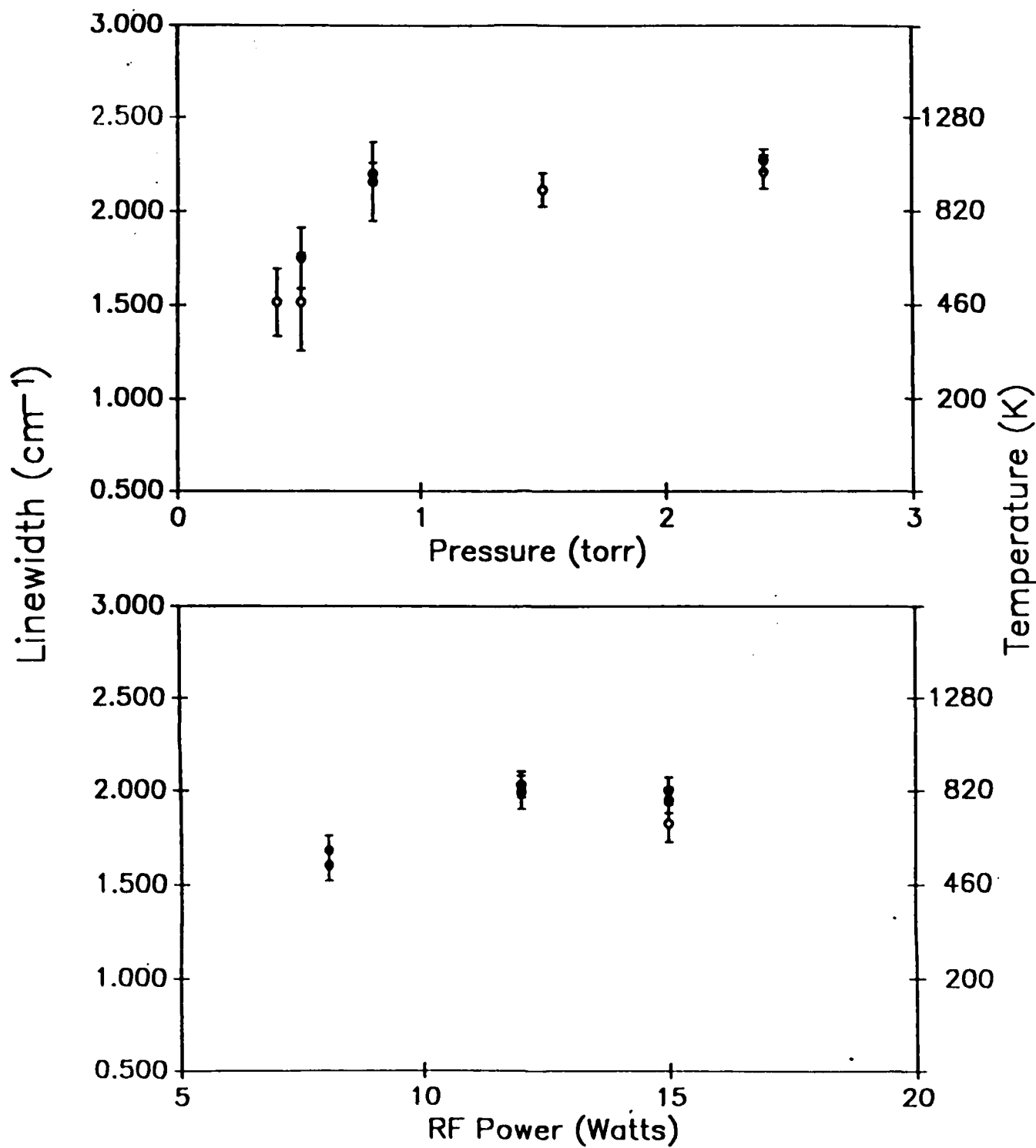


Figure 19. Comparison of linewidth dependence on H₂ pressure (recorded at 12 W RF power) and on discharge power (recorded at an H₂ pressure of 0.42 Torr). Also shown is the temperature scale corresponding to the observed linewidths.

The only possible broadening mechanisms inherent to the RF discharge and exclusive of the microwave discharge would appear to be Stark broadening and Doppler broadening. Both mechanisms also appear consistent with the observed pressure and discharge power dependence. However, Stark broadening appears unlikely because of the fact that D linewidths are narrower by 2.5. Additionally, Stark broadening calculations based on the quasistatic microfield approximation¹⁸ dictate that the electron density in the plasma must be approximately 3 orders of magnitude higher than the 10^{11} electrons/cm³ maintained under typical operating conditions to produce the observed broadening.

The only plausible explanation is Doppler broadening. We propose that H-atoms are being warmed by the charge exchange with hot ionic species in the glow. Donnelly et al.²⁷ have shown that by increasing the power to the discharge, the number of ions increases and then levels out or saturates at higher power. Figure 19 clearly shows a similar phenomena in the linewidth vs. power dependence. The overall temperature varies from approximately 440 to 900K from lower to higher discharge powers. Increasing the pressure also increases the ion density up to a point and then levels off producing similar results for the linewidth as also shown in Fig. 19.

iii) *Ammonia*

In contrast to the above results, translationally hotter hydrogen atoms having a linewidth (see Fig. 20) of approximately 5 cm⁻¹ (fwhm) corresponding to a temperature of ≈ 5000 K, were initially observed while running a pure H₂ RF discharge. However, this discharge was later found to be contaminated by a small leak in the vacuum system. Remarkably, the TALIF signal remained for long periods (1 or 2 h) after the discharge was

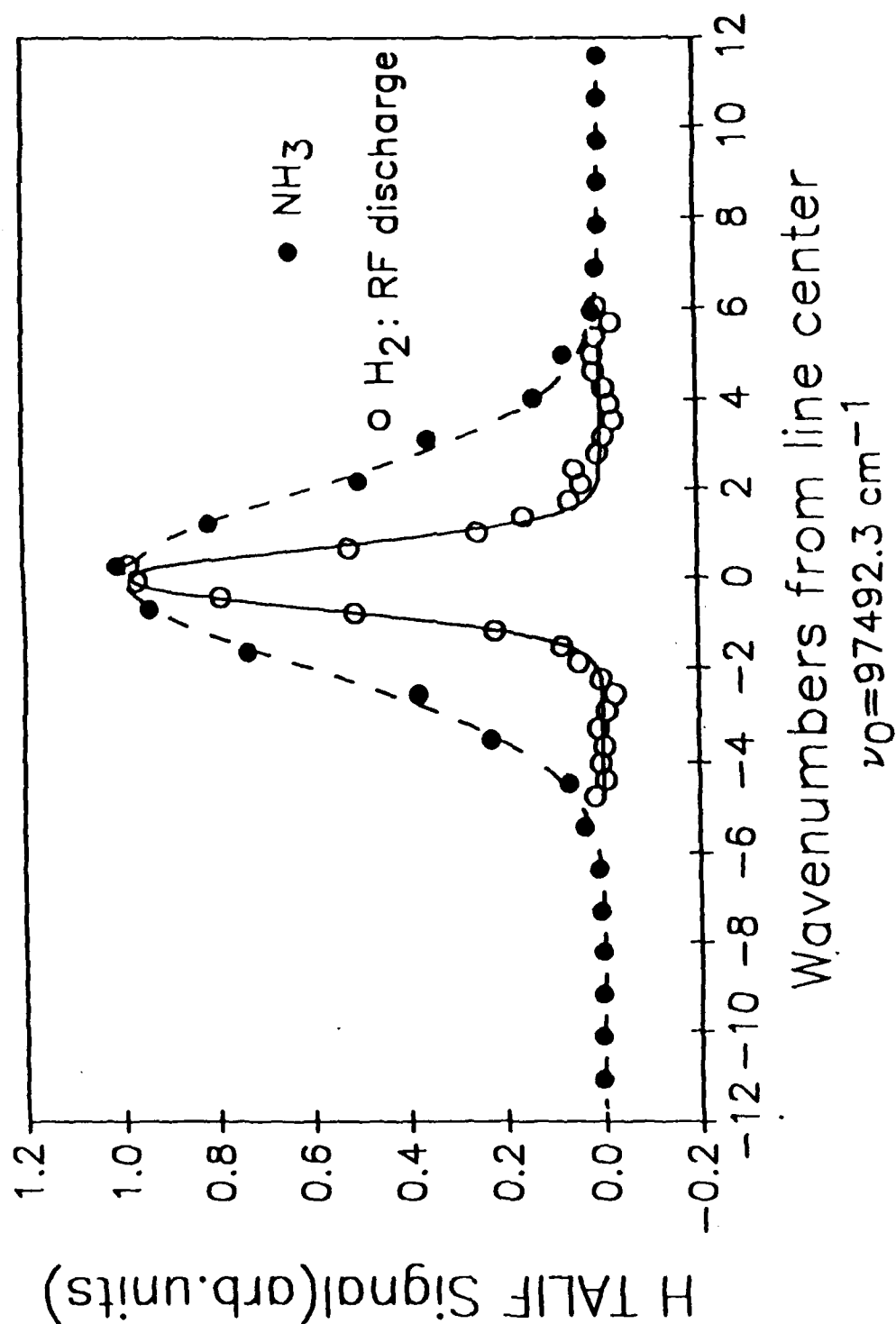


Figure 20. Comparison of the linewidth of RF generated H-atoms (inner trace) and atoms generated from the photodissociation of ammonia. Actual data points and Gaussian fits are shown.

extinguished. It is postulated that H-atoms react with N_2 or N atoms to form NH_3 , which is subsequently photolyzed by one 205-nm photon with the resulting H-atom detected by TALIF. The H-atom would carry translational energy produced by the excess energy of the photolysis laser relative to the N-H bond dissociation energy, D_0 . Photolysis and excitation occur during the same pulse (5 ns), eliminating the possibility of thermalizing collisions.

Earlier work by Back and Koda²⁸ shows that dissociation of NH_3 is easily accomplished by absorption of a photon of 205-nm light to a predissociative state. Results of Uyama and Matsumoto²⁹ show that NH_3 is synthesized in microwave discharges of H_2/N_2 mixtures by formation of NH radicals that further react with either H or H_2 .

Confirmation of the theory of NH_3 synthesis was established by comparison of TALIF linewidths for H_2/N_2 mixtures with TALIF linewidths for NH_3 held static in the cell with the discharge off. Results for TALIF linewidths from hydrogen-nitrogen RF mixtures and pure ammonia (given in Table 1) are identical within experimental error. Additional evidence is shown in Fig. 21, which gives a log plot of H-atom TALIF intensity versus laser power. A slope of two is predicted for TALIF of discharge generated H-atoms, while a slope of three is expected for the three-photon process of photodissociation followed by two-photon absorption. As Fig. 21 shows, the results from the NH_3 experiments indicate a slope close to 3, except at highest laser powers where saturation occurs. It is clear from these data that translationally hot H-atoms are produced by photodissociation of NH_3 .

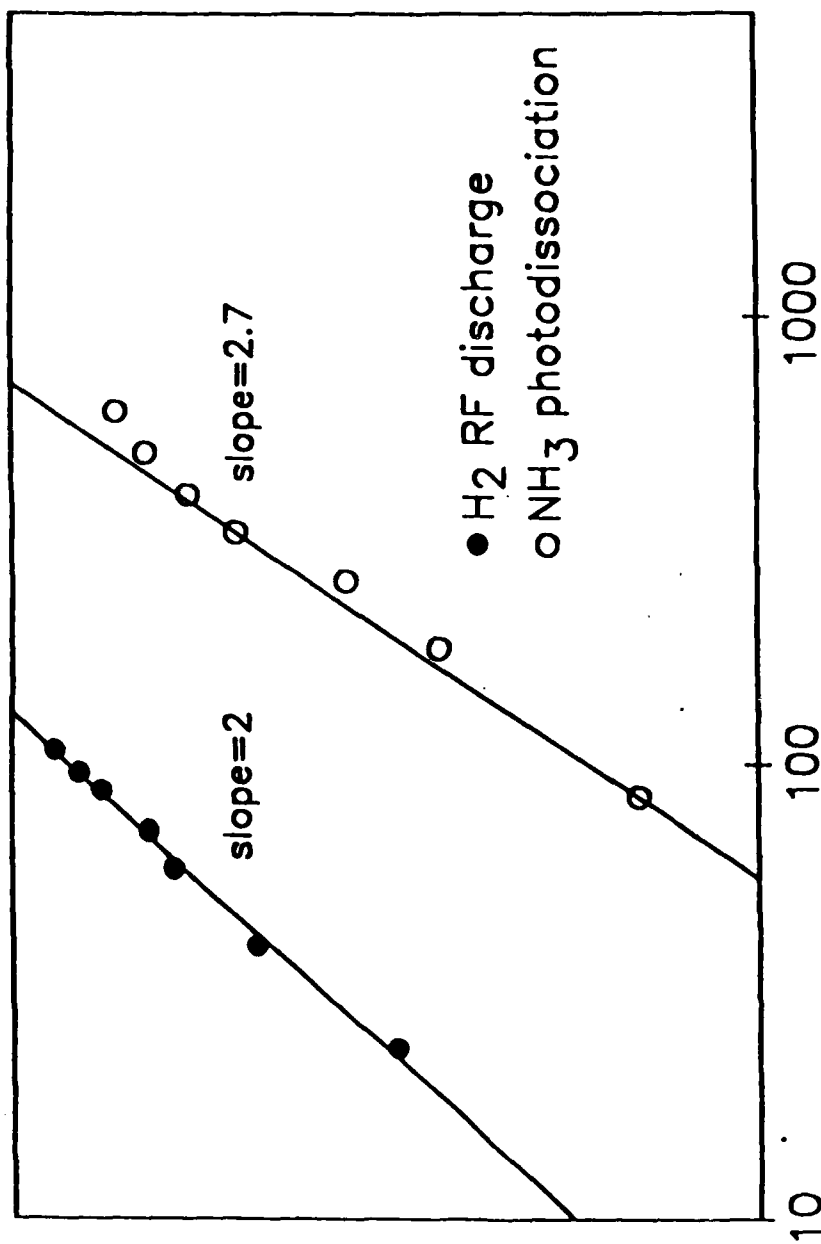
The translational temperature of hot atoms produced photolytically provides a means of identifying the precursor species, via its bond dissociation energy. Segall *et al.*³⁰ demonstrated a technique for measurement of bond dissociation energies from lineshapes of

TABLE 1 Processing Gas Bond Energies and Experimental Linewidths

<u>Gas</u>	<u>Linewidth(cm⁻¹)</u>	<u>Bond Dissociation Energy (kcal/mole)</u>		
		<u>Temperature(K)</u>	<u>This Work</u>	<u>Accepted Value^a</u>
NH ₃	5.01(10)	5150	109(11)	107.4(1.1)
H ₂ S	5.96(14)	7290	94(9)	91.1(1)
H ₂ C ₂	4.48(8)	4100	123(12)	132(5)

^avalues taken from ref. 29.

Log (Intensity)



205-nm power ($\mu\text{J/pulse}$)

Figure 21. Dependence of signal intensity on laser power for RF and photodissociation-generated H-atoms. A slope of 2 is predicted for two-photon TALIF, and a slope of 3 is predicted for the dissociating photon plus the subsequent TALIF detection. Notice the saturation effect at higher laser powers for the NH₃-generated signals.

H-atoms photolyzed from acetylene. This technique yields a controversial result,³¹ but is at worst a good approximation ($\pm 10\%$). The observed lineshape is followed out into the wings to determine maximum kinetic energy of the H-atom. The maximum velocity, v_H^M of the H-atoms contributing to the Doppler profile can be easily related³² to the bond energy, D_0 ,

$$D_0 = E_{205} - E_F = E_{205} - SE_H^M = E_{205} - 1/2 S m_H (v_H^M)^2, \quad (15)$$

where E_F is the energy of all fragments, E_{205} is the photolysis energy, and E_H^M is the maximum energy of the hydrogen atom fragment. The numerical factor S assures conservation of momentum in the photodissociation process. It is entirely determined by the masses of the fragments; for NH_3 , C_2H_2 and H_2S , it is respectively 1.06, 1.08 and 1.03. We have adopted the procedure of fitting the H TALIF lineshape to a Gaussian profile and determining E_H at the 2.5 sigma point on the curve. We were able to derive a bond dissociation energy for $H-NH_2$ of 109 ± 11 kcal/mole which agrees well with the accepted value as shown in Table 1.

iv) *Other Processing Gas Plasmas*

The quality of the determined bond dissociation energy for ammonia led to studies of other processing gases to establish whether they may be identified by lineshape analysis. TALIF signals for hydrogen liberated from H_2S and acetylene were easily obtained and linewidths and bond dissociation energies are also presented in Table 1. Fig. 22 shows the contrast between the lineshapes of H_2C_2 and H_2S generated H-atoms. From Table 1 and Fig. 22, it is clear that the TALIF diagnostic can identify the precursor molecule.

Attempts were also made to observe TALIF signals from photodissociation of methane but were unsuccessful. This is presumably because methane does not possess sufficient

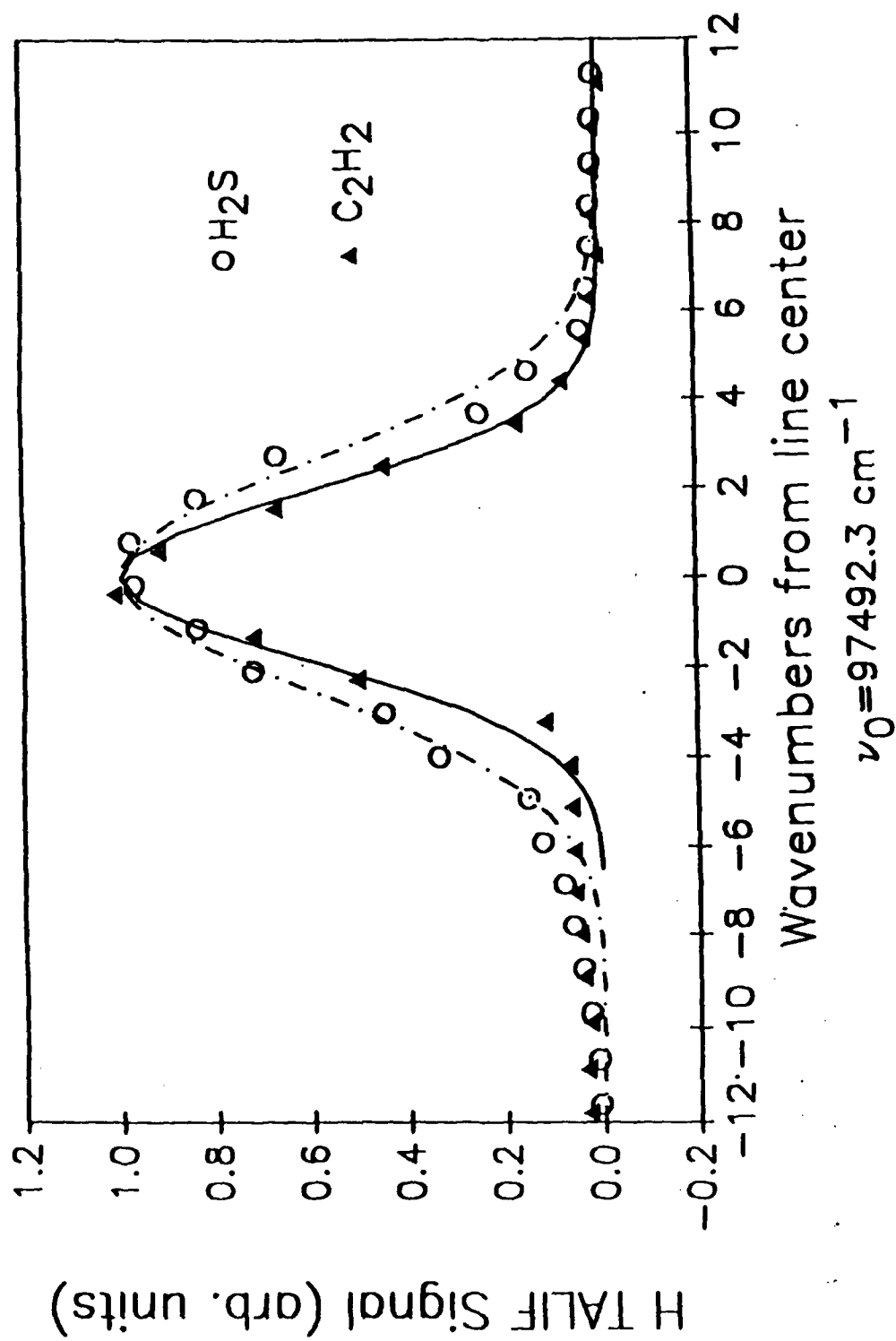


Figure 22. Comparison of the lineshapes for TALIF signals produced from photodissociation of acetylene (triangles) and H_2S .

oscillator strength for absorption of a 205-nm photon, despite the photon having sufficient energy to rupture the C-H bond.^{32,33} The same results were also observed with H₂, presumably for the same reason. This conclusion is strengthened by the almost perfect correlation shown in Fig. 21 between H-atom signal and squared laser power for RF generated H atoms in an H₂ discharge.

While not a perfect method for identifying species in plasma environments, the photodissociation method should prove helpful in this respect. We found that dirty tubing, dirty valves, and even the slightest leaks in our vacuum system, resulted in broadening of our TALIF signals. Thus in a processing reactor with TALIF diagnostic, the width of the H-atom signal can provide a very sensitive indicator of its proper functioning. We have certainly found it to be so with our reactor.

SECTION 4

CONCLUSIONS

We have successfully developed TALIF as a highly spatially and temporally resolved diagnostic of H-atom relative and absolute concentrations in cold, reactive plasmas, such as are commonly used for processing of semiconductors and other materials applications. We have developed a model which accurately accounts for variations of H-atom concentrations both in space and time for plasmas with and without semiconducting wafers present. We have further shown how H-atom TALIF can be used as a sensitive probe of the temperature and purity of the plasma.

These experiments have demonstrated the usefulness of the TALIF diagnostic both as a means for understanding the fundamentals of the discharge and for monitoring plasma processes. It is clear that the TALIF techniques can be extended to monitor other atomic species, O, N, Cl, etc., important in plasma processing. Furthermore, the high spatial resolution should be very useful for probing near-surface interactions. To further generalize the usefulness of the technique, it will be important to extend measurements to higher pressure plasmas. To do this, reliable measurements of quenching crosssections for the fluorescence must be made.

LIST OF REFERENCES

1. U. Niggebrögge, M. Klug, G. Garus, *IOPC Conf. Ser.* **79**, (Karuizawa, Japan) (1985) and D. Lecrosnier, L. Henry, A. LeCorre, C. Vaudray, *Elect. Lett.* **23**, 1254 (1987).
2. S. J. Pearton, J. W. Corbett, and T. S. Shi, *Appl. Phys.* **A43**, 153 (1987). See also R. Gottscho, B. Preppernau, S. Pearton, A. Emerson, and K. Giapis, *J. Appl. Phys.*, **68**, 440 (1990).
3. E. Constant, J. Chevallier, J. C. Pesant, and N. Caglio, *Electron. Lett.* **23**, 841 (1987).
4. G. S. Jackson, N. Pan, M. S. Feng, G. E. Stillman, N. Holonyak, and R. D. Burnham, *App. Phys. Lett.* **51**, 1629 (1987).
5. S. -M. Shin, H. -K. Chung, and K. Tan, *J. Appl. Phys.* **62**, 1729 (1987).
6. K. Bonin and T. McIlrath, "Two-photon electric dipole selection rules," *J. Opt. Soc. Am. B*, **1**, 52 (1984).
7. W. G. ab and J. Hassler, *Applied Optics*, **26**, 3181 (1987).
8. M. Clyre and W. Nip, *Reactive Intermediates in the Gas Phase*, (Academic Press Inc., New York, 1979).
9. J. R. Dunlop, A. D. Tserepi, B. L. Preppernau, T. M. Cerny, and T. A. Miller, *Plasma Chem. Plasma Process* **12**, 1 (1992).
10. B. L. Preppernau and T. A. Miller, "Laser-Based Diagnostics of Reactive Plasmas," in *Glow Discharge Spectroscopy*, edited by R. K. Marcus (Plenum, New York, NY, 1993).
11. A. Hines and R. Maddox, *Mass Transfer, Fundamentals and Applications* (Prentice Hall, Englewood Cliffs, NJ, 1985).
12. P. R. Wallace, *Mathematical Analysis of Physical Problems* (Dover New York, 1984).
13. S. G. Hansen, G. Luckman, G. C. Nieman, and S. D. Colson, *Appl. Phys. Lett.* **56**, 719 (1990).
14. G. S. Selwyn, *J. Appl. Phys.* **60**, 2771 (1986).
15. R. A. Gottscho and M. L. Mandich, *J. Vac. Sci. Technol. A* **3**, 617 (1985).
16. S. G. Hansen, G. Luckman, G. C. Nieman, and S. D. Colson, *J. Appl. Phys.* **68**, 2013 (1990).

17. A. D. Tserepi, J. R. Dunlop, B. L. Preppernau, and T. A. Miller, *J. Appl. Phys.* **72**, 2638 (1992).
18. H. Wise and B. J. Wood, *Adv. At. Mol. Phys.* **3**, 291 (1967).
19. A. Bouchoule, C. Laure, P. Ranson, Dj. Salah, and D. Henry, Proceedings for the 5th Symposium on Plasma Processing, 1984 (unpublished).
20. A. Bouchoule and P. Ranson, *J. Vac. Sci. Technol. A* **9**, 317 (1991).
21. A. L. Cappelli, R. A. Gottscho, and T. A. Miller, *Plasma Chem. Plasma Process.* **5**, 317 (1985).
22. R. S. Freund, J. A. Schiavone, and D. F. Biader, *J. Chem. Phys.* **64**, 1122 (1976).
23. J. A. Schiavone, K. C. Smyth, and R. S. Freund, *J. Chem. Phys.* **63**, 1043 (1975).
24. T. Ogawa, J. Kurawaki, and M. Higo, *Chem. Phys.* **61**, 181 (1981).
25. M. Higo, S. Kaurata, and T. Ogawa, *Chem. Phys.* **66**, 243 (1982).
26. M. D. Harmony, *Introduction to Molecular Energies and Spectra*, Holt, Rinehart, and Winston, New York (1972).
27. V. M. Donnelly, D. L. Flamm, and G. Collins, *J. Vac. Sci. Technol.* **21**, 817 (1992).
28. R. A. Back and S. Koda, *Can. J. Chem.* **55**, 1387 (1977).
29. H. Uyama and O. Matsumoto, *Plasma Chem. Plasma Process.* **9**, 421 (1989).
30. J. Segall, R. Lavi, Y. Wen, and C. Wittig, *J. Phys. Chem.* **93**, 7287 (1989).
31. T. A. Miller, *CHEMTRACTS-Anal., Phys., Inorg. Chem.* **2**, 187 (1990).
32. G. Herzberg, *Electronic Spectra of Polyatomic Molecules*, (Van Nostrand Reinhold., Cincinnati, (1966).
33. D. F. McMillen and D. M. Golden, *Annu. Rev. Phys. Chem.* **88**, 493 (1982).

APPENDIX

Publications

1. "Temporally Resolved Laser Diagnostic Measurements of Atomic Hydrogen Concentrations in RF Plasma Discharges," B. L. Preppernau, D. A. Dolson, R. A. Gottscho, and T. A. Miller, *Plasma Chem. and Plasma Proc.* **9**, 157 (1989).
2. "Enhanced Atomic Hydrogen Concentration Measurements in RF Discharges," B. L. Preppernau and T. A. Miller, *J. Vac. Sci. Tech.*, **A8**, 1673 (1990).
3. "Laser-Based Diagnostics of Reactive Plasmas," B. L. Preppernau and T. A. Miller, in *Glow Discharge Spectroscopies*, R. K. Marcus, ed., (Plenum, New York, NY, 1993).
4. "H-Atom Plasma Diagnostics: A Sensitive Probe of Temperature and Purity," J. R. Dunlop, A. D. Tserepi, B. L. Preppernau, T. M. Cerny, and T. A. Miller, *Plasma Chem. Plasma Proc.*, **12**, 1 (1992).
5. "The Effects of Surfaces on H-Atom Concentration in Pulsed and Continuous Discharges," A.D. Tserepi, J.R. Dunlop, B.L. Preppernau and T.A. Miller, *J. Vac. Sci. & Tech.*, **10**(4), 1188, (1992).
6. "Absolute H-Atom Concentration Profiles in Continuous and Pulsed RF Discharges," A.D. Tserepi, J.R. Dunlop, B.L. Preppernau and T.A. Miller, *J. Appl. Phys.*, **72**(7), 2638, (1992).

Presentations

1. "Atomic Hydrogen Measurements in Hydrogen-Bearing Plasmas," B. L. Preppernau, A. D. Tserepi, T. Cerny, and T. A. Miller, 42nd Annual Gaseous Electronics Conference, Menlo Park, CA, October 17-20, 1989.
2. "Enhanced Atomic Hydrogen Concentration Measurements in RF Discharges," B. L. Preppernau and T. A. Miller, 36th National Symposium of the American Vacuum Society, Boston, MA, October 23-27, 1989.
3. "Applications of Atomic Hydrogen Detection by Two-Photon Laser Induced Fluorescence," B. L. Preppernau, A. Tserepi, J. R. Dunlop, T. Cerny, and T. A. Miller, Society for Applied Spectroscopy, Columbus, OH, February 9, 1990.
4. "Lineshape Measurements in Processing Gas Discharges," J. R. Dunlop, T. M.

- Cerny, B. L. Preppernau, A. D. Tserepi, and T. A. Miller, 43rd Annual Gaseous Electronics Conference, Champaign-Urbana, IL, October 17-19, 1990.
5. "Calibrated Spatial and Temporal Profiles of H-Atoms in Hydrogen Discharges," B. L. Preppernau, T. M. Cerny, J. R. Dunlop, A. D. Tserepi, and T. A. Miller, 43rd Annual Gaseous Electronics Conference, Champaign-Urbana, IL, October 17-19, 1990.
 6. "An Overview of III-V and Diamond Processing Diagnostics at The Ohio State University," T.A. Miller, Wright Patterson Air Force Base, Dayton, OH, May 30, 1991.
 7. "Spatial Profiles of Absolute H-atom Concentration in RF Discharges," A. D. Tserepi, J.R. Dunlop, B.L. Preppernau, and T.A. Miller, G.E.C. 91, Albuquerque NM, 22-25 October, 1991.
 8. "Hydrogen Plasmas in the Presence of III-V Materials," A.D. Tserepi, J.R. Dunlop, B.L. Preppernau, T.A. Miller, American Vacuum Society, Boston, MA, November 11-15, 1991.
 9. "Effects on surfaces on H-atom Concentration Profiles in Continuous and Pulsed Discharges," A.D. Tserepi, B.L. Preppernau, J.R. Dunlop, T.A. Miller, Evans Lecture, Ohio State University, Poster Session, November 1991.
 10. "Measurement of Atomic Hydrogen Concentration Profile in GEC Reference Cell," B.L. Preppernau, and T.A. Miller, 45th Annual Gaseous Electronics Conference, Boston, MA, October 27-30, 1992.
 11. "Spatially and Temporally Resolved Detection of H Atoms in RF Plasmas," A.D. Tserepi, and T.A. Miller, 45th Annual Gaseous Electronics Conference, Boston, MA, October 27-30, 1992.
 12. "Spatially and Temporally Resolved Profiles of O Atoms in Etching Plasmas," A.D. Tserepi, and T.A. Miller, 45th Annual Gaseous Electronics Conference, Boston, MA, October 27-30, 1992.